Inorganic Chemistry

Article

pubs.acs.org/IC

DNA/Protein Binding, Molecular Docking, and in Vitro Anticancer Activity of Some Thioether-Dipyrrinato Complexes

Rakesh Kumar Gupta,[†] Gunjan Sharma,[‡] Rampal Pandey,[†] Amit Kumar,[†] Biplob Koch,[‡] Pei-Zhou Li,[§] Qiang Xu,[§] and Daya Shankar Pandey*[,†]

[†]Department of Chemistry, and [‡]Department of Zoology, Faculty of Science, Banaras Hindu University, Varanasi, 221 005 Uttar Pradesh, India

[§]National Institute of Advanced Industrial Science and Technology (AIST), 1-8-31, Midorigaoka, Ikeda, Osaka 563-8577, Japan

Supporting Information

ABSTRACT: Syntheses and characterizations of the arene ruthenium [(η^6-C_6H_6)RuCl(4-mtdpm)] (**1**), [(η^6-*p*-$MeC_6H_4Pr^i$)RuCl(4-mtdpm)] (**2**), and structurally analogous rhodium/iridium complexes [(η^5-C_5Me_5)RhCl(4-mtdpm)] (**3**) and [(η^5-C_5Me_5)IrCl(4-mtdpm)] (**4**) [4-mtdpm = 5-(4-methylthiophenyl)-dipyrromethene] have been reported. Their identities have been established by satisfactory elemental analyses, electrospray ionization-mass spectrometry (ESI-MS), FT-IR, NMR (^{1}H, ^{13}C), UV/vis, emission spectral, and electrochemical studies. Structure of the representative complex **3** has been authenticated by X-ray single crystal analyses. The complexes **1**−**4** effectively bind with calf thymus DNA (CT DNA) through intercalative/electrostatic interactions. In addition, these exhibit significant cytotoxicity toward Dalton lymphoma (DL) cell line and cause static quenching of the bovine serum albumin (BSA) fluorophore. The antiproliferative activity, morphological changes, and apoptosis have been evaluated by MTT assay, acridine orange/ethidium bromide (AO/EtBr) fluorescence staining, and DNA ladder assay. Mode of interaction of the complexes with DNA/protein has also been supported by molecular docking. Various studies revealed remarkable decrease in the in vitro DL cell proliferation and induction of the apoptosis by **1**−**4**, which lies in the order **2** > **1** > **4** > **3**.

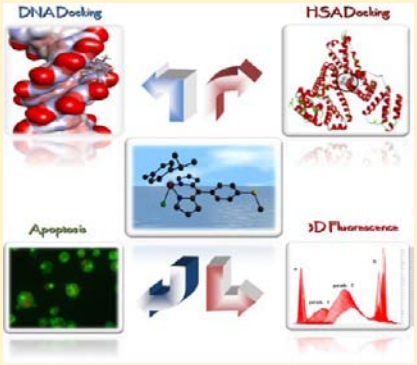

INTRODUCTION

Cancer is one of the most fatal diseases in the world posing serious health problems to humanity and causes the death of millions of people every year.[1] Therefore exploration of the anticancer drugs has emerged as an essential area in pharmaceutical research.[2] In this milieu the metal complexes capable of binding/cleaving DNA and proteins, and exhibiting catalytic activity toward glutathione have drawn enormous current interest.[3] Among these, platinum based anticancer drug *cis*-platin and its analogues have proved to be indispensable in cancer chemotherapy; however, they are associated with high toxicity, drug selectivity, and resistivity.[4] The drawbacks associated with platinum based drugs have prompted chemists to investigate more efficient, less toxic, and target specific anticancer drugs derived from other metals.[5] In this direction, ruthenium has drawn particular attention because of its diverse characteristics and a variety of significant roles in biological systems.[6] In quest of the potential anticancer drug candidates numerous ruthenium complexes have been synthesized and extensively investigated, among these KP1019 and NAMI-A are very promising and have entered in clinical trials.[7] Owing to their wide structural diversity and bonding modes organometallic half-sandwich arene ruthenium and structurally analogous pentamethylcyclopentadienyl rhodium/iridium complexes have offered great promise.[8] Consequently the designing and synthesis of new organometallic complexes based on Ru(II), Rh(III), and Ir(III) exhibiting DNA/protein binding, cleavage, and catalytic activity toward glutathione are highly desirable.[9]

At the same time, proteins have also attracted enormous research interest as a prime molecular target.[10] Serum albumins such as bovine serum albumin (BSA) is the most important protein present in plasma that carries several endo- and exogenous compounds.[10] It is essential to explore drug−protein interactions as most of the drugs bound to serum albumin are usually transported as a protein complex.[11] Attention has also been focused on the proteins that drive and control cell cycle progression.[12] Apart from the DNA and protein binding the organometallic half-sandwich ruthenium, rhodium, and iridium complexes also exhibit catalytic anticancer activity and can increase intracellular reactive oxygen species (ROS).[13] The ROS level is attenuated by glutathione (GSH) which is a major endogenous antioxidant and directly participates in the neutralization of free radicals and ROS.

Further, dipyrrins are highly sought-after molecules because of their unique characteristics, ability to form stable neutral/anionic homo/heteroleptic dipyrrinato complexes with several

Received: June 29, 2013
Published: November 27, 2013

metal ions and applicability in diverse areas.[14,15] Recently, we reported some half-sandwich Ru(II), Rh(III), and Ir(III) complexes containing 4-(2-methoxypyridyl)phenyldipyrromethene (2-pcdpm) and their DNA binding, in vitro cytotoxicity, and antitumor activity on DL cell lines.[9d] It is well-known that sulfur is an important constituent of biomolecules and plays a crucial role in biological systems.[16] In addition, it has been shown that sulfur containing compounds exhibit good DNA/protein binding/cleaving and catalytic activity toward glutathione.[13,17] To explore the role of thioether moiety in DNA binding/cleavage activity of the half-sandwich ruthenium, rhodium, and iridium dipyrrinato complexes, 5-(4-methylthiophenyl)dipyrromethene (4-mtdpm) was chosen as a ligand for the present study. The incorporation of thioether moiety may (i) enhance the possibility of stacking and intercalation, (ii) the noncovalent interaction of the planar thioether dipyrrin core with DNA/proteins, and (iii) alter the catalytic oxidation of thiols, cysteine/glutathione and, in turn, cytotoxicity and antitumor activity of the ensuing complexes.

Through this contribution we describe the synthesis and characterization of complexes $[(\eta^6\text{-}C_6H_6)RuCl(4\text{-mtdpm})]$ (**1**), $[(\eta^6\text{-}p\text{-}MeC_6H_4Pr^i)RuCl(4\text{-mtdpm})]$ (**2**), $[(\eta^5\text{-}C_5Me_5)RhCl(4\text{-mtdpm})]$ (**3**), and $[(\eta^5\text{-}C_5Me_5)IrCl(4\text{-mtdpm})]$ (**4**) imparting 5-(4-methylthiophenyl)dipyrromethene. Also, we describe herein the interaction of **1**−**4** with CT DNA/protein, supported by UV/vis, fluorescence, synchronous, and 3D-fluorescence spectroscopy, molecular docking studies, and in vitro anticancer activity toward DL cells.

EXPERIMENTAL SECTION

Reagents. Reagent grade chemicals were used throughout, solvents dried and distilled following the literature procedures, and reactions were carried out under nitrogen atmosphere.[18] Metal chlorides ($RuCl_3{\cdot}xH_2O$, $RhCl_3{\cdot}xH_2O$, $IrCl_3{\cdot}xH_2O$), agarose, 1,3-cyclohexadiene, 2,3-dichloro-5,6-dicyano-1,4-benzoquinone (DDQ), 4-(methylthio)-benzaldehyde, pentamethylcyclopentadiene, α-terpinene (α-phellandrene), and pyrrole were procured from Sigma Aldrich Chemical Co., and used without further purifications. 3-(4,5-Dimethylthiazol-2-yl)-2,5-diphenyltetrazolium bromide (MTT), RPMI-1640, and DNA Ladder as Marker (200−2000 bp) were purchased from Hi-Media, ethylenediaminetetraacetic acid (EDTA) and ethidium bromide (EtBr) from Loba Chemie, while acridine orange (AO) from Sisco Research Laboratory (SRL), Mumbai, India. Calf thymus (CT) DNA was purchased from Bangalore Genei, India. The precursor complexes $[\{(\eta^6\text{-arene})Ru(\mu\text{-}Cl)Cl\}_2]$ (η^6-arene = C_6H_6, p-$MeC_6H_4Pr^i$), $[\{(\eta^5\text{-}C_5Me_5)M(\mu\text{-}Cl)Cl\}_2]$ (M = Rh or Ir) were prepared and purified following literature procedures.[19]

General Methods. Elemental analyses (C, H, and N), spectral [FT-IR, UV/vis, NMR ^{1}H (300 MHz) and ^{13}C (75.45 MHz)] and electrochemical data on the complexes were obtained as described elsewhere.[9d] Fluorescence spectra was acquired on a LS-55 Spectrofluorimeter (Perkin-Elmer, U.K.) equipped with a xenon lamp in a 10.0 mm quartz cell. The excitation and emission slit widths were set at 10.0 and 5.0 nm, respectively, and temperature was maintained by recycling water using a Peltier system. The electrospray ionization-mass spectrometry (ESI-MS) data was obtained on a Bruker Daltonics Amazon SL ion trap mass spectrometer. Samples were dissolved in 100% acetonitrile with 0.1% formic acid and introduced into the ESI source through a syringe pump at a flow rate 100 μL/h. The capillary voltage was 4500 V, dry gas flow 8 L/min, and dry gas temperature 300 °C. The MS scan was acquired for 2.0 min, and spectra printouts were averaged of over each scan.

Synthesis of $[(\eta^6\text{-}C_6H_6)RuCl(4\text{-mtpm})]$ (1). DDQ (0.227 g, 1.0 mmol) dissolved in benzene (15 mL) was added dropwise with stirring to an ice cooled solution of 5-(4-methylthiophenyl)dipyrromethane (4-mtdpmH, 0.267 g, 1.0 mmol) dissolved in CH_2Cl_2 (40 mL) over a period of 30 min. After complete consumption of the starting material (monitored by TLC), the solvent was evaporated under reduced pressure and the resulting residue redissolved in CH_2Cl_2/MeOH (50 mL; 1:1 v/v) and filtered to remove any solid impurities. Triethylamine (1.0 mL) and $[\{(\eta^6\text{-}C_6H_6)Ru(\mu\text{-}Cl)Cl\}_2]$ (0.250 g, 0.50 mmol) were successively added to the clear filtrate and stirred for an additional ∼4 h at room temperature (rt). The reaction mixture was concentrated to dryness under reduced pressure and crude product purified by column chromatography (Silica gel, CH_2Cl_2 with 1% MeOH) to afford complex **1** as a red solid. Yield: 54% (0.259 g). Anal. Calc for $C_{22}H_{19}N_2ClSRu$, requires: C, 55.05; H, 3.99; N, 5.84. Found C, 55.16; H, 4.06; N, 5.69%. ^{1}H NMR ($CDCl_3$, δ ppm): 2.54 (s, 3H, $SC\underline{H}_3$), 5.27 (s, 6H, $C_6\underline{H}_6$), 6.41 (d, 2H, J = 3.6 Hz, pyrrolic), 6.61 (d, 2H, J = 3.9 Hz, pyrrolic), 7.29 (m, 4H, phenyl), 8.15 (s, 2H, pyrrolic). ^{13}C NMR ($CDCl_3$, δ ppm): 15.15 ($S\underline{C}H_3$), 86.47, ($\underline{C}_6H_6$), 117.90, 124.72, 130.91, 131.22, 133.15, 139.17, 146.00, 153.12. ESI-MS. (Calcd, found, m/z) 445.0, 445.2 $[M-Cl]^+$. IR (KBr pellets, cm^{-1}): 727, 811, 986, 997, 1031, 1249, 1342, 1375, 1529, 1557. UV/vis: (c, 10 μM; EtOH:H_2O, 1:1, v:v; pH ∼7.3; λ_{max} nm, ε M^{-1} cm^{-1}): 490 (2.96 × 10^4), 427 (1.49 × 10^4), 251 (3.23 × 10^4).

Synthesis of $[(\eta^6\text{-}p\text{-}MeC_6H_4Pr^i)RuCl(4\text{-mtdpm})]$ (2). This complex was prepared following the above procedure for **1** except that $[\{(\eta^6\text{-}p\text{-}MeC_6H_4Pr^i)Ru(\mu\text{-}Cl)Cl\}_2]$ (0.306 g, 0.50 mmol) was used in place of $[\{(\eta^6\text{-}C_6H_6)Ru(\mu\text{-}Cl)Cl\}_2]$. Yield: 59% (0.316 g). Anal. Calc for $C_{26}H_{27}N_2ClSRu$: requires: C, 58.25; H, 5.08; N, 5.23. Found: C, 58.20; H, 5.13; N, 5.47%. ^{1}H NMR ($CDCl_3$, δ ppm): 1.07 (d, 6H, J = 7.9 Hz, $CH_3C_6H_4CH(C\underline{H}_3)_2$), 2.28 (s, 3H, $C\underline{H}_3C_6H_4$−$CH(CH_3)_2$), 2.43 (m, 1H, $CH_3C_6H_4C\underline{H}(CH_3)_2$), 2.54 (s, 3H, $SC\underline{H}_3$), 5.28 (s, 4H, $CH_3C_6\underline{H}_4CH(CH_3)_2$), 6.47 (d, 2H, J = 4.2 Hz, pyrrolic), 6.62 (d, 2H, J = 4.2 Hz, pyrrolic), 7.30 (m, 4H, phenyl), 8.01 (d, 2H, J = 8.4 Hz, pyrrolic). ^{13}C NMR ($CDCl_3$, δ ppm): 15.40 ($CH_3C_6H_4CH$-$(\underline{C}H_3)_2$), 18.50 ($\underline{C}H_3C_6H_4CH(CH_3)_2$), 21.99 ($CH_3C_6H_4\underline{C}H(CH_3)_2$), 30.47 ($S\underline{C}H_3$), 84.49, 84.73, 100.15, 101.91 (($CH_3\underline{C}_6H_4CH(CH_3)_2$), 118.22, 124.74, 130.78, 134.51, 134.99, 139.05, 145.79, 154.69. ESI-MS. (Calcd, found, m/z) 501.1, 501.2, $[M-Cl]^+$. IR (KBr pellets, cm^{-1}): 726, 810, 987, 998, 1032, 1249, 1341, 1375, 1530, 1556. UV/vis: (c, 10 μM; EtOH:H_2O, 1:1, v:v; pH ∼7.3; λ_{max} nm, ε M^{-1} cm^{-1}): 489 (2.66 × 10^4), 416 (1.12 × 10^4), 255 (2.52 × 10^4).

Synthesis of $[(\eta^5\text{-}C_5Me_5)RhCl(4\text{-mtdpm})]$ (3). It was prepared following the above procedure for **1** using $[\{(\eta^5\text{-}C_5Me_5)Rh(\mu\text{-}Cl)Cl\}_2]$ (0.309 g, 0.50 mmol) in place of $[\{(\eta^6\text{-}C_6H_6)\text{-}Ru(\mu\text{-}Cl)Cl\}_2]$. Yield: 54% (0.323 g). Microanalytical data: $C_{27}H_{32}N_2ClSRh$, requires: C, 58.43; H, 5.81; N, 5.05. Found C, 58.63; H, 5.73; N, 5.25%. ^{1}H NMR ($CDCl_3$, δ ppm): 1.48 (s, 15H, $C_5(C\underline{H}_3)_5$), 2.57 (s, 3H, $SC\underline{H}_3$), 6.44 (s, 2H, pyrrolic), 6.54 (s, 2H, pyrrolic), 7.35 (s, 4H, phenyl), 7.66 (s, 2H, pyrrolic). ^{13}C NMR ($CDCl_3$, δ ppm): 8.30 $C_5(\underline{C}H_3)_5$), 15.37 ($S\underline{C}H_3$), 96.46 ($\underline{C}_5(CH_3)_5$), 117.89, 125.32, 130.70, 131.49, 133.17, 135.60, 139.83, 146.41, 153.21. ESI-MS (Calcd, found, m/z): 503.1, 503.2 $[M-Cl]^+$. IR (KBr pellets, cm^{-1}): 769, 804, 991, 1021, 1251, 1340, 1374, 1533, 1556. UV/vis: (c, 10 μM; EtOH:H_2O, 1:1, v:v; pH ∼7.3; λ_{max} nm, ε M^{-1} cm^{-1}): 501 (3.49 × 10^4), 389 (1.84 × 10^4), 253 (3.01 × 10^4).

Synthesis of $[(\eta^5\text{-}C_5Me_5)IrCl(4\text{-mtdpm})]$ (4). It was synthesized following the above procedure for **1** using $[\{(\eta^5\text{-}C_5Me_5)Ir(\mu\text{-}Cl)Cl\}_2]$ (0.309 g, 0.50 mmol) instead of $[\{(\eta^6\text{-}C_6H_6)\text{-}Ru(\mu\text{-}Cl)Cl\}_2]$. Yield: 55% (0.378 g). Microanalytical data: $C_{27}H_{32}N_3ClSIr$, requires: C, 50.33; H, 5.01; N, 4.35. Found: C, 50.25; H, 5.17; N, 4.25%. ^{1}H NMR ($CDCl_3$, δ ppm): 1.47 (s, 15H, $C_5(C\underline{H}_3)_5$), 2.54 (s, 3H, $SC\underline{H}_3$), 6.47 (d, 2H, J = 7.2 Hz, pyrrolic), 6.70 (d, 2H, J = 3.9 Hz, pyrrolic), 7.31 (m, 4H, phenyl), 7.77 (s, 2H, pyrrolic). ^{13}C NMR ($CDCl_3$, δ ppm): 8.34 ($C_5(\underline{C}H_3)_5$), 15.41 ($S\underline{C}H_3$), 94.41, 94.50 ($\underline{C}_5(CH_3)_5$), 118.83, 124.81, 130.63, 132.45, 134.50, 135.62, 139.18, 145.88, 152.85. ESI-MS (Calcd, found, m/z): 593.2, 593.3 $[M-Cl]^+$. IR (KBr pellets, cm^{-1}): 803, 989, 1019, 1251, 1338, 1372, 1531, 1555. UV/vis: (c, 10 μM; EtOH:H_2O, 1:1, v:v; pH ∼7.3; λ_{max} nm, ε M^{-1} cm^{-1}): 499 (2.95 × 10^4), 387 (1.49 × 10^4), 254 (2.43 × 10^4).

X-ray Structure Determination. Single crystal X-ray analysis on **3** was performed on a R-AXIS RAPID II diffractometer using Mo−Kα radiation (λ = 0.71073 Å) at the single crystal X-ray diffraction center,

Scheme 1. Synthesis of Complexes 1−4

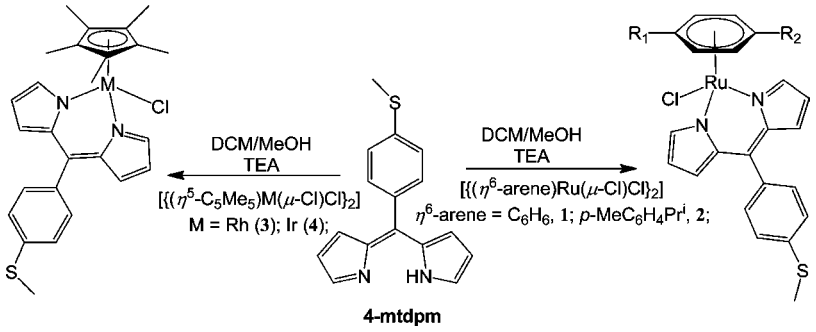

National Institute of Advanced Industrial Science and Technology (AIST), Osaka, Japan. The structure was solved by direct methods (SHELXS 97) and refined by full-matrix least-squares on F^2 (SHELX 97).[20] All the non-H atoms were treated anisotropically. The H-atoms attached to carbon were included as a fixed contribution and were geometrically calculated and refined using the SHELX riding model. The computer program PLATON was used for analyzing the interaction and stacking distances.[21] CCDC deposition No. 928847 (**3**) contains the supplementary crystallographic data for this paper. The data can be obtained free of charge via http://www.ccdc.cam.ac.uk/conts/retrievinghtml (or from the CCDC, 12 Union Road, Cambridge CB2 1EZ, U.K.; Fax: +44−1223−336033; E-mail: deposit@ccdc.cam.ac.uk).

DNA Interaction Studies. Electronic absorption (10 μM, EtOH/H_2O, 1:1, v/v) and electrochemical titrations (CH_3CN, 100 μM) were carried out using a fixed concentration of the complexes and increasing the concentration of CT DNA (Na-phosphate buffer solution, pH ∼7.2) following an earlier procedure.[9d] Ethidium bromide (EtBr) displacement experiments were performed by monitoring changes in the fluorescence intensity at excitation and emission wavelengths (λ_{ex}, 525; λ_{em} 602 nm) after aliquot addition of **1−4** to an aqueous solution of the EtBr-DNA.

Protein Binding Studies. In protein binding studies the excitation and emission wavelengths of BSA at 280 and ∼348 nm were monitored using BSA (0.5 μM) solution prepared in Tris-HCl buffer (pH ∼7.5), and the solution was stored in a dark place at 4 °C. Synchronous fluorescence spectral studies were performed at two different $\Delta\lambda$ values (difference between the λ_{ex} and λ_{em} of BSA) such as 15 and 60 nm, using similar concentration of the BSA and compounds. The 3D-fluorescence spectra were acquired under the following conditions: the emission wavelength was in the range 200−500 nm; the initial excitation wavelength was set to 200 nm with increments of 5 nm; the number of total scans was 31, and other parameters were the same as those for fluorescence quenching spectra.

Partition Coefficient Determination. Lipophilicity of the complexes under study were evaluated by the "Shake flask" method in octanol/water phase partitions as mentioned elsewhere.[9d,22]

Molecular Docking. Molecular docking studies on **1−4** have been performed using HEX 6.1 software and Q-site finder which is an interactive molecular graphics program for the interaction, docking calculations, and to identify possible binding site of the biomolecules.[23] The density functional theory (DFT) calculations were carried out using the GAUSSIAN03 program and the B3LYP method. The geometries of the complexes under study were optimized using standard 6-31G** basis sets for N, C, H, S, and Cl elements and LANL2DZ for Ru, Rh, and Ir with effective core pseudo potentials for these metal atoms.[24] The coordinates of metal complexes were taken from their optimized structure as a .mol file and were converted to .pdb format using CHIMERA 1.5.1 software. The crystal structure of B-DNA (PDB ID: 1BNA) and human serum albumin (PDB ID: 1h9z) were retrieved from the protein data bank (http://www.rcsb.org./pdb). Visualization of the docked systems has been performed using Discovery Studio 3.5 software. The by default parameters were used for the docking calculation with correlation type shape only, FFT mode at 3D level, grid dimension of 6 with receptor range 180 and ligand range 180 with twist range 360 and distance range 40.

Cell Viability and Proliferation Assay/MTT Assays. The cell viability and proliferation was evaluated by MTT [3-(4,5-dimethylthiazol-2-yl)-2,5-diphenyltetrazoliumbromide] assay.[25] To estimate the cell viability and proliferation, DL cells were seeded at 2.5×10^4 cells/well in RPMI-1640 medium with 10% Fetal Bovine Serum (FBS) in 96-well plates. Seeded DL cells were treated with increasing concentration of complexes **1−4** dissolved in dimethylsulfoxide (DMSO) and diluted with RPMI-1640 (the concentration of DMSO did not exceed 0.1% v/v) and incubated for 24 h. The volume of treated (0.1% v/v DMSO) and control well were kept the same in this study. After incubation, the cells were washed with PBS and MTT was added (*c*, 0.5 μg/mL). These were again incubated for 2 h at 37 °C and to ensure the formation of MTT crystals and then dissolve in DMSO (100 μL). After 30 min the absorbance (570 nm) was measured using an ELISA plate reader. The results are expressed as percentage of the cell viability with respect to control. Dose response curves were obtained by plotting percent cell survival (percent control) vs drug concentration. Percent control was calculated using the following formula:

$$\%\text{Control} = [\text{Mean O. D. of the Drug treated well} / \text{Mean O. D. of the control well}] \times 100$$

Morphological Analysis by Acridine Orange (AO) and Ethidium Bromide (EtBr) Staining. The DL cells (1×10^6 in number) were cultured in 6 well plates at 37 °C in an incubator in RPMI-1640 medium with L-glutamine supplemented with antibiotics and 10% FBS and treated with increasing concentration of **1−4** (5, 10 μg/mL) for 24 h. The cells were harvested and washed with PBS, and 40 μL of AO/EtBr solution (1 part of 100 μg/mL of AO in PBS; 1 part of 100 μg/mL of EtBr in PBS) was added. After staining the cells were washed with PBS twice, suspended in 200 μL of PBS, and cell morphology examined under a fluorescence microscope. The images were photographed by Nikon 800 fluorescence microscope at 40× resolution.

This technique is used to distinguish viable cells, early apoptotic cells with blebbing, and necrotic cells.[26] Acridine orange intercalates into the DNA and gives a green fluorescence and thus the viable cells appear with a green nucleus while early apoptotic cells with a condensed or fragmented nuclei. Ethidium bromide is taken up only by the non-viable cells giving a bright orange nucleus of the dead cells overwhelming the acridine orange stain.[27]

DNA Fragmentation Assay. The cell death may take place either by apoptosis (programmed cell death) or by necrotic cell death. In apoptosis the cleavage of DNA takes place into internucleosomal fragments of ∼180 base pairs (bp) and its multiple (360, 540, etc.).[28] Total nuclear DNA was isolated from DL cells following the procedure described by Kuo et al.[29] The DL cells were seeded in 6 well plates and treated with **1−4** at different concentrations (2, 5, and 10 μg/mL) for 24 h in RPMI-1640 medium with 10% FBS. The cells were washed twice with PBS and treated with lysis buffer [20 mM Tris-HCl (pH ∼7.5), 0.15 M NaCl, 1 mM EDTA, 0.5% SDS] at 4 °C for 30 min. After centrifugation (3,000 rpm, 10 min, rt), 25 μL of the proteinase K

(stock 20 mg/mL) was added to the supernatant and incubated for 2 h at 37 °C. It was centrifuged (12,000 rpm, 4 °C for 30 min), chilled absolute ethanol, and 0.1 M NaCl were successively added to the supernatant for DNA precipitation. Precipitated DNA was thoroughly washed with 70% ethanol, dried, and dissolved in autoclaved distilled water. DNA fragmentation was visualized by electrophoresis in 1.8% agarose gel containing ethidium bromide and photographed in a Gel documentation system (G: BOX, SYNGENE).

RESULTS AND DISCUSSION

Synthesis and Characterization. The ligand 4-mtdpmH was prepared by condensation of 4-(methylthio)benzaldehyde with an excess of pyrrole in the presence of catalytic amount of trifluoroacetic acid (TFA) following the method described by Cohen et al.[30] Desired complexes $[(\eta^6\text{-}C_6H_6)RuCl(4\text{-mtdpm})]$ (**1**), $[(\eta^6\text{-}p\text{-}MeC_6H_4Pr^i)RuCl(4\text{-mtdpm})]$ (**2**), $[(\eta^5\text{-}C_5Me_5)RhCl(4\text{-mtdpm})]$ (**3**), and $[(\eta^5\text{-}C_5Me_5)IrCl(4\text{-mtdpm})]$ (**4**) were obtained in good yields (54−59%) by treatment of the chloro- bridged dimeric ruthenium $[\{(\eta^6\text{-arene})Ru(\mu\text{-}Cl)Cl\}_2]$ (η^6-arene = C_6H_6, p-$MeC_6H_4Pr^i$) and rhodium/iridium complexes $[\{(\eta^5\text{-}C_5Me_5)M(\mu\text{-}Cl)Cl\}_2]$ [M = Rh, Ir] with in situ generated 4-mtdpm obtained by oxidation of 4-mtdpmH with DDQ in presence of triethylamine at rt. A simple scheme showing the synthesis of **1**−**4** is given below (Scheme 1).

The complexes under investigation are crystalline, non hygroscopic solids, stable at rt, and soluble in common organic solvents such as methanol, ethanol, benzene, chloroform, dichloromethane, acetone, dimethylsulfoxide, dimethylformamide, and insoluble in hexane, petroleum ether, and diethyl ether. These have been characterized by satisfactory elemental analyses, ESI-MS, IR, ^{1}H, ^{13}C NMR, UV/vis spectral and electrochemical (CV and DPV studies. The molecular structure of **3** has been determined crystallographically.

In their IR spectra **1**−**4** exhibited intense bands due to $\nu(C{=}N_{pyr})$ at (1557, **1**; 1556, **2**; 1556, **3**; 1555 cm^{-1}, **4**) in conjunction with other bands associated with dipyrrin moieties. IR spectral data supported coordination of the dipyrrin ligand and formation of respective complexes.[9d,14] Information about the composition and stability of **1**−**4** have also been obtained from ESI-MS spectral studies. In their ESI-MS spectra the complexes exhibited a strong peak due to $[M-Cl]^+$ (m/z 445.3 **1**; 501.2, **2**; 503.2, **3**; 591.3, **4**). Notably, **1**−**4** do not show a molecular ion peak; rather these exhibit a peak due to $[M-Cl]^+$ suggesting that chloro group is highly labile (Supporting Information, Figure S1−S4).

NMR Spectral Studies. ^{1}H and ^{13}C NMR spectral data for **1**−**4** are summarized in the Experimental Section, and resulting spectra depicted through Supporting Information, Figures S5−S8. It was observed that the protons associated with 4-mtdpm in **1** and **2** exhibited an appreciable downfield shift relative to the free ligand[30] and resonated at δ ~2.54, S−CH_3; 6.46 (β−pyrrolic); 6.61 (β−pyrrolic), 7.30 (phenyl), and 8.00 ppm (α−pyrrolic).[9d,14] Downfield shift in the position of pyrrolic protons may be attributed to interaction of the 4-mtdpm with the ruthenium center. The η^6-C_6H_6 protons in **1** displayed an upfield shift and appeared at δ 5.27 ppm relative to the precursor complex,[9d,14] while the η^6-p-$MeC_6H_4Pr^i$ ring protons in **2** resonated at δ 1.07, $[CH(CH_3)_2]$, 2.23, C−CH_3, 2.43, $[CH(CH_3)_2]$ and 5.28 ppm (merged peak, C_6H_4).[9d,14] On the other hand, protons due to the ligand 4-mtdpm in **3** and **4** displayed a small upfield shift [δ ~2.54, S−CH_3, 6.47 (β−pyrrolic); 6.70 (β−pyrrolic); 7.30 (phenyl) and 7.77 ppm (α−pyrrolic)] relative to the 4-mtdpmH, and *Cp** ring protons exhibited an insignificant shift in comparison to the respective precursor complexes [δ 1.48, **3**; and 1.47 ppm, **4**]. NMR data of the complexes strongly supported coordination of the ligand 4-mtdpm to the metal center which has been verified by structural studies on the representative complex **3**. ^{13}C NMR spectral data of **1**−**4** also supported formation of the respective complexes and are comparable with the earlier reports.[9d,14,31]

Crystal Structure. The structure of complex **3** has been determined by X-ray single crystal analyses. It crystallizes in the monoclinic system with $P2_1/c$ space group. Details about the data collection, solution, and refinement are gathered in the Experimental Section and Table 1. The molecular structure along with a partial atom numbering scheme is shown in Figure 1, and important bond lengths and angles are summarized in Table 2. The Rh(III) center in this complex adopted typical piano stool geometry with two positions occupied by pyrrolic nitrogen (N1, N2) from 4-mtdpm; the chloro (Cl1) group and *Cp** ring bonded in η^5-manner. The rhodium to pyrrolic nitrogen bond distances are identical [Rh−N1, 2.08 Å; Rh−N2, 2.08 Å], while Rh−Cl bond distance (Rh−Cl1) is 2.40 Å; these distances are normal and comparable to those of other closely

Table 1. Crystal Data and Structure Refinement Parameters for 3

empirical formula	$C_{27}H_{30}Cl_3RhN_2S$
crystal system	monoclinic
space group	$P2_1/c$
a (Å)	8.975(2)
b (Å)	22.519(5)
c (Å)	14.075(3)
α (deg)	90.00
β (deg)	101.92(3)
γ (deg)	90.00
V (Å^3), Z	2783.3(10), 4
λ (Å)	0.71073
color and habit	Red, block
T (K)	153(2)
reflns collected	25905
refins/restraint/params	6341/0/313
D_{calcd} (Mg m^{-3})	1.489
μ (mm^{-1})	0.995
GOF on F^2	1.018
final R indices $I > 2\sigma(I)$	R1 = 0.0668
	wR2 = 0.1543
R indices (all data)	R1 = 0.0991
	wR2 = 0.1723

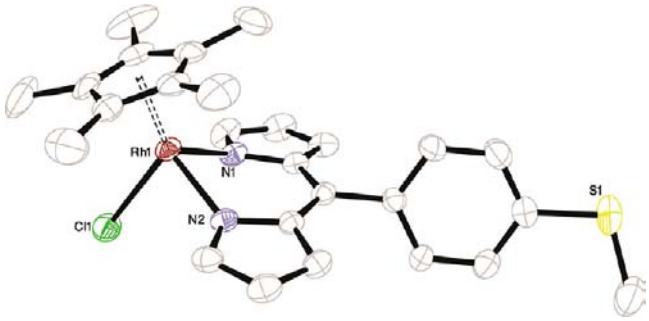

Figure 1. ORTEP view of **3** at 30% thermal ellipsoid probability (H-atoms omitted for clarity).

dx.doi.org/10.1021/ic401662d | Inorg. Chem. 2013, 52, 13984−13996

Table 2. Selected Bond Lengths (Å) and Angles (deg) for 3[a]

	3
Bond Length (Å)	
Rh−N1	2.08(5)
Rh−N2	2.08(5)
Rh−Cl1	2.40(17)
C23−S1	1.77(7)
C26−S1	1.75(10)
Rh−C*g*	1.79
Rh−C*av*	2.16
Bond Angle (deg)	
N2−Rh1−N1	84.30(18)
N2−Rh1−Cl1	90.60(14)
N1−Rh1−Cl1	90.87(14)
C23−S1−C26	105.3(4)
ω	69.86

[a]*Cg* = metal centroid bond distance, *Cav* = average metal−carbon bond distance, ω = the twist angle between dipyrrin core and *meso*-phenyl substituent.

related complexes.[9d,14,31] The bond angles N−Rh−N and N−Rh−Cl about the metal center are close to 90° [N1−Rh−N2, 84.30°; N1−Rh−Cl1, 90.60°; N2−Rh−Cl1, 90.87°] (Table 2). The *Cp** ring is symmetrically bonded to the metal ion with an average Rh−C bond distances of 2.16 Å [range, 2.135−2.175 Å]. The *Cp** ring is planar, and the separation between the rhodium and the centroid of the *Cp** ring is 1.79 Å. This distance is consistent with the values reported in other related systems.[9d,14,31] The dihedral angle between *meso*-phenyl substituent and dipyrrin moiety is normal (69.86°) and in agreement with other reports.[9d,14,31]

Electronic Absorption Spectroscopy. UV/vis. spectra of **1**−**4** were acquired in aqueous medium (EtOH:H_2O, *c*, 10 μM; 1:1, v/v; pH ∼7.3) and resulting data is given in the Experimental Section. Strong low energy absorptions at ∼490 nm [490, **1**; 489, **2**; 501, **3**; 499 nm **4**] and weak bands [427, **1**; 416, **2**; 389, **3**; 387 nm **4**] in the spectra of complexes may be attributed to S0−S1 and S0−S2 transitions of the conjugated dipyrrinato ligand.[9d,14,15] These also displayed high energy intense bands at ∼250 nm [251, **1**; 255, **2**; 253, **3**; 254 nm **4**], which have been ascribed to the intraligand $\pi-\pi^*$ transitions (Figure 2).[9d,14,15]

UV/vis Titration Studies. To understand the mode of interaction of complexes with CT DNA, absorption titration studies have been performed by monitoring the changes in absorption intensity by aliquot addition of DNA.[32] Usually, intercalation between the metal complexes and DNA results in hypochromism with or without red/blue shift;[33] on the other hand, non-intercalative/electrostatic interaction causes hyperchromism.[34] The absorption spectra of **1**−**4** in absence and presence of CT DNA is depicted in Figure 3 (Supporting Information, Figure S9). From the absorption titration spectrum (Figure 3) it is apparent that upon addition of CT DNA (2 μM) to a solution of **1** the intra ligand band (251 nm) displayed hyperchromism (ε, 0.321 × 10^5−0.379 × 10^5 M^{-1} cm^{-1}) along with a negligible red shift (∼252 nm). On the other hand bands at 427 and 490 nm exhibited hypochromism (ε, 0.149 × 10^5−0.156 × 10^5 M^{-1} cm^{-1}, 427 nm; 0.296 × 10^5−0.298 × 10^5 M^{-1} cm^{-1}, 490 nm) without any significant shift. An increase in the concentration of CT DNA (3−20 μM) causes hyperchromism (ε, 0.759 × 10^5 M^{-1} cm^{-1}) for the band at 251 nm with a red shift of ∼2 nm (∼253 nm). On the contrary, the band at 427 nm showed hypochromism (ε, 0.128 × 10^5 M^{-1} cm^{-1}), and the one at 490 nm displayed hypochromism (ε, 0.281 × 10^5 M^{-1} cm^{-1}) with a small blue shift of ∼2 nm (∼488 nm). The isosbestic point at ∼345 nm in the titration curve indicated presence of more than two species in the medium. An analogous spectral pattern has been observed for **2** (Supporting Information, Figure S9a).

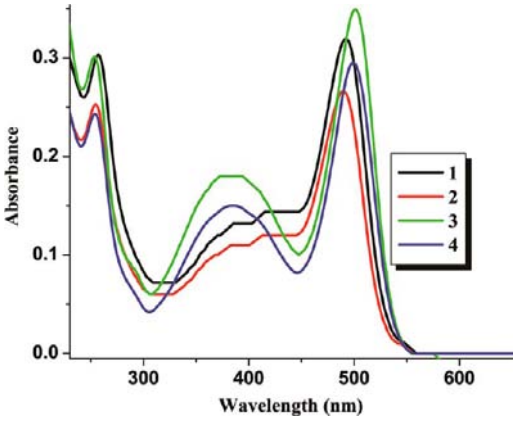

Figure 2. Electronic spectra of **1**−**4** in (EtOH:H_2O, *c*, 10 μM; 1:1, v/v; pH ∼7.3).

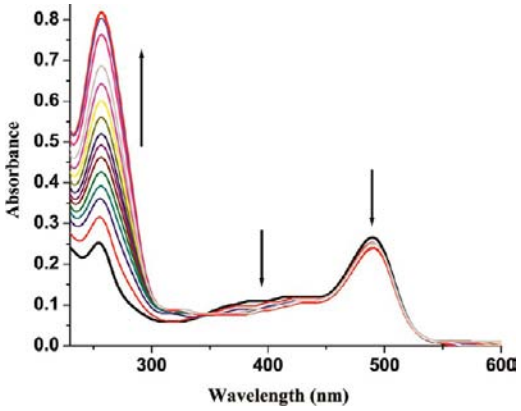

Figure 3. Absorption titration spectra of **1** (EtOH:H_2O, *c*, 10 μM; 1:1, v/v; pH ∼7.3) in the absence (black line) and presence (other lines) of CT DNA to complex (1−20 μM) at rt. Arrow shows the absorbance changes upon increasing CT DNA concentration.

Complexes **3** and **4** exhibited slightly different behavior relative to those of **1** and **2**. The band at 253 nm showed a hyperchromic shift (ε, 0.301 × 10^5−0.335 × 10^5 M^{-1} cm^{-1}) with an insignificant red shift upon addition of the CT DNA (2 μM) to a solution of **3**. The band at 389 nm exhibited hypochromism (ε, 0.182 × 10^5−0.179 × 10^5 M^{-1} cm^{-1}) without any noteworthy shift; however, the one at 501 nm displayed hyperchromism (ε, 0.349 × 10^5−0.354 × 10^5 M^{-1} cm^{-1}) with a small blue shift. Further aliquot addition of CT DNA (3−20 μM) resulted in hyperchromism for the band at 253 nm (ε, 0.629 × 10^5 M^{-1} cm^{-1}) with a red shift of ∼3 nm (∼256 nm). Conversely, the band at 389 nm displayed hypochromism (ε, 0.162 × 10^5 M^{-1} cm^{-1}) and hyperchromism at 501 nm (ε, 0.392 × 10^5 M^{-1} cm^{-1}). Although the former did not show any shift in the position of the band, the latter displayed a blue shift of ∼4 nm (∼497 nm). The presence of more than two species in the medium was indicated by the isosbestic points at ∼502, 445, 369 nm (Supporting

dx.doi.org/10.1021/ic401662d | *Inorg. Chem.* 2013, 52, 13984−13996

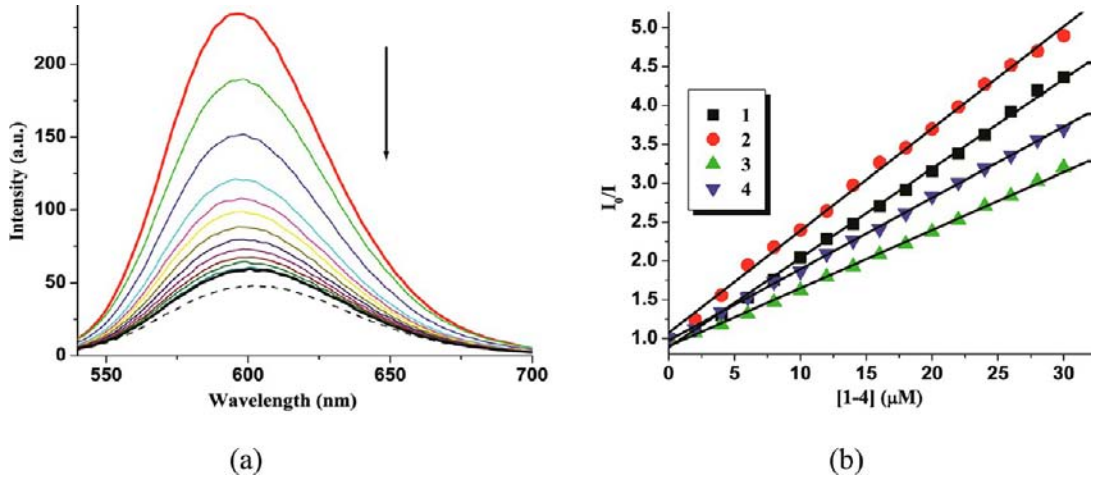

Figure 4. Emission spectra of EtBr (black dotted line), EtBr bound to the DNA (Red solid line), and in the presence (other lines) of **2** with increasing amounts 0−50 μM (a). [EtBr] = 10 μM, [DNA] = 10 μM. Arrow shows changes in the emission intensity upon addition of the increasing complex concentration. Stern−Volmer plots of the EtBr-DNA fluorescence titration for complexes **1**−**4** (b).

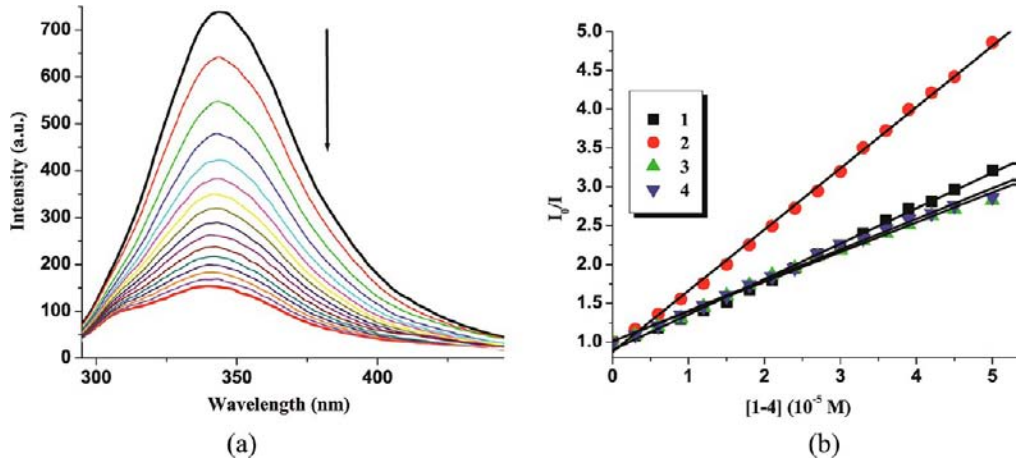

Figure 5. Emission spectrum of BSA (black line) (0.5 μM; λ_{ex} = 280 nm; λ_{em} = 343 nm) in presence (other lines) of **2** with increasing amounts (0−50 μM) (a), Arrow shows the emission intensity changes upon increasing complex concentration. Stern−Volmer plots of the fluorescence titrations of **1**−**4** (b).

Information, Figure S9b). An analogous spectral pattern was observed for **4** also under similar condition (Supporting Information, Figure S9c). The absorption titration studies suggested definitive interaction between complexes under investigation and CT DNA. Further, on the basis of hypo/hyperchromism of the intense low energy band, we concluded that the mode of interaction of **3** and **4** is different from those of **1** and **2**.

To compare the binding affinity of the complexes with CT DNA, equilibrium binding constants (K_b) and binding site size (s, per base pair) were worked out using Bard's equation based on the McGhee−von Hippel (MvH) model.[35] The calculated intrinsic equilibrium binding constants (K_b) and binding site size (s) (2.3×10^{-5}, 0.13, **1**; 8.9×10^{-5}, 0.14, **2**; 6.3×10^{-4}, 0.12, **3**; 7.4×10^{-4}, 0.13, **4**) are comparable to the earlier reports (Supporting Information, Table S3).[36] Absorption titration studies clearly suggested rather strong binding of **2** with CT DNA, and the binding affinity of **1**−**4** falls in the order **2** > **1** > **4** > **3**. The higher binding affinity of **2** may be due to steric hindrance enforced by the bulkier p-$MeC_6H_4Pr^i$ moiety. Further, low values of s suggested the groove binding and/or surface binding.

Ethidium Bromide (EtBr) Displacement Studies. Absorption titration studies indicated that **1**−**4** effectively bind with DNA. To have deep insight into the nature of bonding and binding affinities, EtBr displacement experiments have been performed.[37] The displacement of EtBr from a DNA sequence in presence of a quencher leads to a decrease in the fluorescence intensity and forms the basis of displacement technique. The quenching phenomenon arises because of the decrease in the number of binding sites on the DNA available for EtBr. Emission spectra of the EtBr and DNA bonded EtBr in the absence and presence of **1**−**4** is depicted in Figure 4 (Supporting Information, Figure S10). An increase in the concentration of **1**−**4** leads to hypochromism with red shift (73%, 4, **1**; 74%, 7, **2**; 68%, 3, **3**; 70%, 6 nm, **4**) relative to initial fluorescence intensity. It suggested that EtBr molecules are displaced from the DNA binding sites by complexes under investigation.[38] Quenching parameters were analyzed following the Stern−Volmer equation.

$$I_0/I = Kq[Q] + 1$$

where I_0 and I are the emission intensities in absence and presence of the quencher, Kq is the quenching constant, and

dx.doi.org/10.1021/ic401662d | Inorg. Chem. 2013, 52, 13984−13996

[Q] presents concentration of the complex. The *K*q values have been derived from the slope of the plot of I_0/I vs [Q] and are (1.15×10^4, **1**; 1.35×10^5, **2**; 7.47×10^4, **3**; 9.17×10^4, **4**). Further, apparent DNA binding constants (K_{app}) were calculated using the eqn:

$$K_{EtBr}[EtBr] = K_{app}[complex]$$

where, [complex] is the value at 50% decrease in the fluorescence intensity of EtBr, K_{EtBr} (1.0×10^7 M^{-1}) is the DNA binding constant of EtBr, and [EtBr] is the concentration of EtBr (10 μM). The K_{app} values for **1**−**4** were found to be (1.18×10^6, **1**; 2.36×10^6, **2**; 7.15×10^5, **3**; 8.42×10^5 M^{-1}, **4**). From the above data it is clear that **2** replaces EtBr more effectively relative to other complexes which is in agreement with the results obtained from electronic absorption studies. From the observed quenching and binding parameters we conclude that all the complexes bind DNA via intercalation mode.

Protein Binding Studies. Interaction between the most abundant blood protein, that is, serum albumin, and complexes have attracted immense current interest because of their structural homology with human serum albumin.[39] To understand the mechanism of interaction between **1**−**4** and BSA, fluorescence quenching experiments have been carried out. The fluorescence properties of BSA arise from intrinsic characteristics of the proteins, mainly due to presence of tryptophan and tyrosine residues. Alteration in the emission spectra arises primarily from the tryptophan residue because of protein conformational changes, subunit association, substrate binding, or denaturation.[40] Therefore, fluorescence behavior of BSA can provide significant information about the structure, dynamics, and protein folding. Fluorescence titration studies have been performed at rt using 0.5 μM BSA and varying the concentration of **1**−**4** (0−50 μM) in the range 290−500 nm (λ_{ex}. 280 nm, Figure 5 and Supporting Information, Figure S11). The fluorescence intensity of BSA at ∼343 nm quenched with a small blue shift (69.12%, 2, **1**; 79.06%, 3, **2**; 59.73%, 2, **3**; and 62.23%, 4 nm, **4**). The blue shift primarily arises due to the presence of the active site of the protein in a hydrophobic environment. It suggested that some interaction is taking place between the complexes and the BSA protein.[40]

The quenching mechanism may follow either static or dynamic mode. Static quenching usually results from the formation of a complex between quencher and fluorophore in the ground state, whereas in dynamic quenching the fluorophore and quencher get in touch with each other during the transient existence of the excited state.[39,40] One can easily distinguish between the dynamic and static quenching by following their temperature dependence. In dynamic quenching high temperature results in quicker diffusion and therefore the quenching rate constant increases with increasing temperature. On the other hand, in static quenching an increase in the temperature reduces stability of the complex, and the quenching constant (Supporting Information, Figure S12 and Table S4) shows that K_{SV} decreases with increasing temperature. It suggested that BSA fluorescence quenching occurs via a static quenching mechanism.[39,40]

The UV/vis absorption spectrum of BSA (fluorophore) offers a simple and an easy means to explore the type of quenching. For a dynamic quenching appreciable change in absorption spectra of the fluorophore is not expected; in contrast, static quenching usually leads to perturbation of the fluorophore.[39,40] The absorption intensity of BSA increases with a small blue shift of about ∼2 nm (Figure 6) and suggested static interaction between BSA and **1**−**4**.

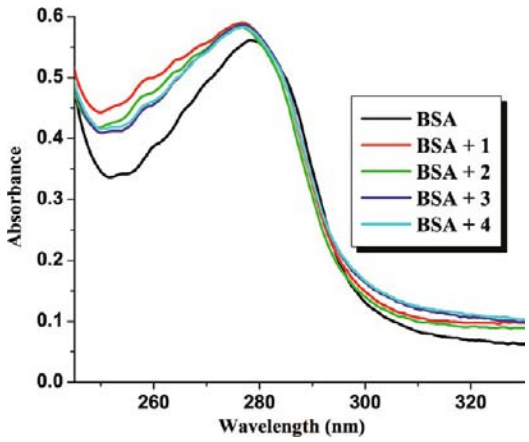

Figure 6. UV/vis absorption spectra of BSA ((Tris-HCl buffer, *c*, 10 μM, pH ∼7.5) in the presence of **1**−**4** (5 μM).

To have a deep insight into the quenching progression, quenching constant (K_q) was evaluated following Stern−Volmer and Scatchard equation using I_0/I vs [Q] plot (Figure 5b). Further, the equilibrium binding constant was also evaluated using the Scatchard equation:

$$\log[(I_0 - I)/I] = \log K_{bin} + n \log [Q]$$

where K_{bin} is binding constant of the compound with BSA and *n* is number of binding sites. From the log $(I_0-I)/I$ vs log [Q] plot, the binding constant (K_{bin}) and the number of binding sites (*n*) have been calculated (Supporting Information, Table S4). Evaluated values of the K_q, K_{bin}, and *n* are gathered in Supporting Information, Table S4. For all the compounds, the estimated value of *n* (∼1) strongly supported the existence of a single binding site in BSA for **1**−**4**. The values of K_q and K_{bin} for these compounds further suggested that **2** interact with BSA rather strongly relative to other complexes under investigation.

Conformational Investigation. The difference between the excitation and the emission wavelength ($\Delta\lambda = \lambda_{ex}-\lambda_{em}$) gives an idea about the type of the chromospheres in BSA.[41] The use of $\Delta\lambda$ 15 nm gives synchronous fluorescence spectrum characteristic of tyrosine whereas $\Delta\lambda$ 60 nm for tryptophan residues.[42] Emission maxima of the tryptophan and tyrosine residues of the protein are related to the polarity of their surroundings. The synchronous fluorescence spectra of BSA with varying concentrations of **1**−**4** acquired at $\Delta\lambda$ = 15 nm and $\Delta\lambda$ = 60 nm are shown in Figure 7 (Supporting Information, Figure S13−S14).

In the synchronous fluorescence spectra at $\Delta\lambda$ = 15 nm addition of the complexes **1**−**4** to a solution of BSA (Tris-HCl buffer, pH ∼7.5) displayed decrease in fluorescence intensity of the band at 288 nm (46.79, **1**; 57.37, **2**; 42.93, **3**; 44.96%, **4**) with an insignificant blue shift of 1 or 2 nm. However, synchronous fluorescence spectra at $\Delta\lambda$ = 60 nm led to a decrease in the fluorescence intensity of the band at 280 nm (72.27, **1**; 86.77, **2**; 67.63, **3**; and 74.83%, **4**). The quenching in fluorescence intensity of the tyrosine and tryptophan residues are indicative of conformational changes, an increase in the hydrophobicity, and decrease in their polarity.[42] The results suggested that **1**−**4** effectively bind with BSA and can be utilized for anticancer activity.

dx.doi.org/10.1021/ic401662d | *Inorg. Chem.* 2013, 52, 13984−13996

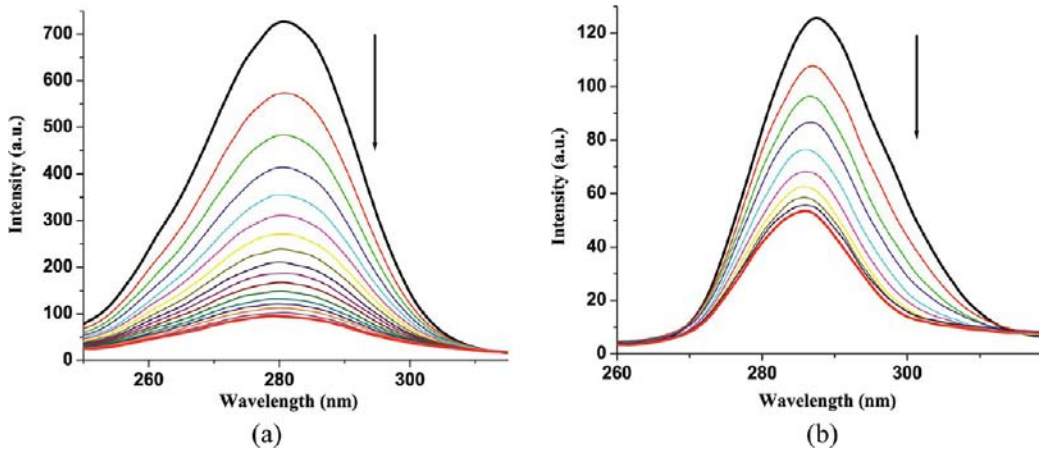

Figure 7. Synchronous spectra of BSA (black line) (Tris-HCl buffer, c, 0.5 μM, pH ~7.5) in presence (other lines) of **2** with increasing amounts (0–50 μM) with wavelength difference of (a) $\Delta\lambda$ = 60 nm **2** (b) $\Delta\lambda$ = 15 nm. Arrows show the emission intensity decrease accompanied by blue shift upon the increasing concentration.

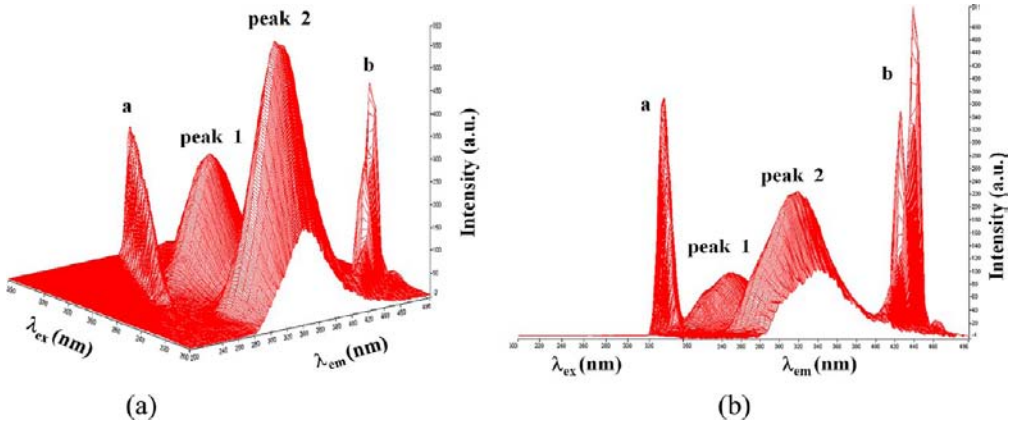

Figure 8. 3D fluorescence spectra of BSA (Tris-HCl buffer, pH ~7.5) (a) and BSA + **2** (b). c(BSA) = 2 × 10^{-6} mol L^{-1}, c(**2**) = 2 × 10^{-6} mol L^{-1}.

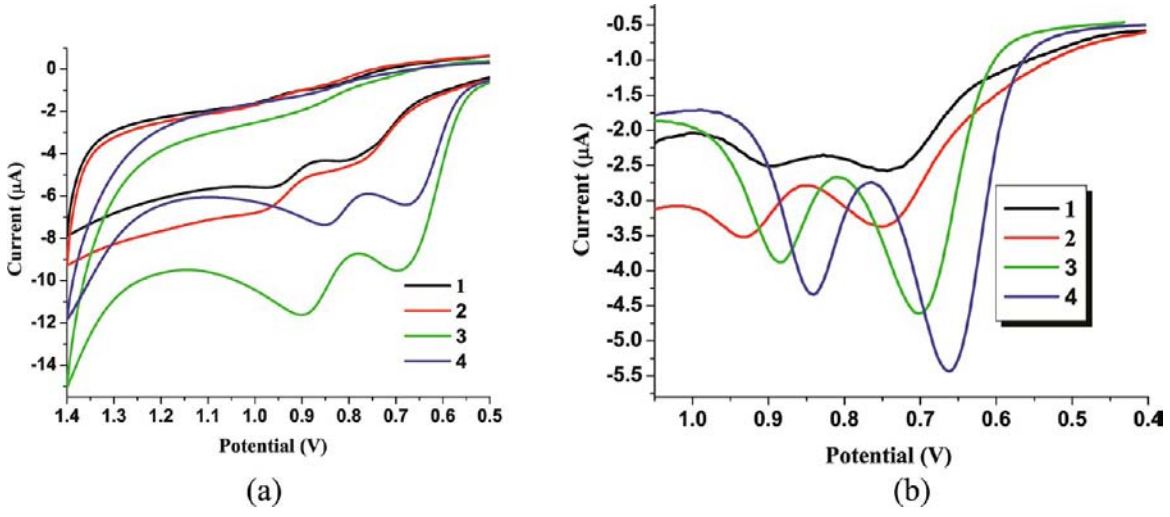

Figure 9. Cyclic (a) and differential pulse voltammograms (b) of **1**–**4** in MeCN (c, 100 μM).

Three Dimensional (3D) Fluorescence Spectroscopy. Excitation Emission Matrix Spectroscopy (EEMS) or three-dimensional (3D) fluorescence spectroscopy is another powerful tool to analyze the microenvironment and conformational changes about BSA.[43] The 3D fluorescence spectrum of BSA and BSA in presence of **1**–**4** is depicted in Figure 8 (Supporting Information, Figure S15) and resulting data collected in Supporting Information, Table S5. It exhibited four characteristic peaks; the extreme left one has been assigned as the first order Rayleigh scattering peak whose emission wavelength matches well with excitation wavelength ($\lambda_{em} = \lambda_{ex}$) whereas the peak on extreme right as second order Rayleigh

dx.doi.org/10.1021/ic401662d | Inorg. Chem. 2013, 52, 13984–13996

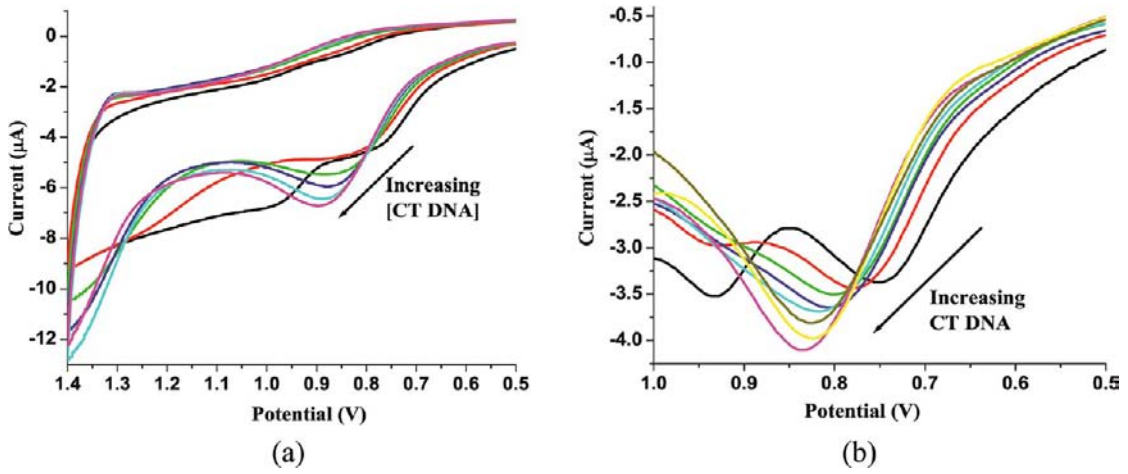

Figure 10. Evolution of the CV (a) and DPV (b) of **1** (*c*, 100 μM, MeCN) in absence (black) and presence (other lines) of increasing the amounts CT DNA (0.0−1.0 μM), at rt.

scattering peak ($\lambda_{em} = 2\lambda_{ex}$) marked as "a" and "b", respectively (Figure 8). In addition, there are two additional peaks denoted as "peak 1" and "peak 2". The peak 1 revealed spectral behavior of tyrosine and tryptophan residues, whereas 2 displayed fluorescence behavior of the polypeptide backbone and secondary structure of the protein.[44]

These results showed that peak 1 did not exhibit any significant shift whereas it displayed significant decrease in the intensity (69, **1**; 72, **2**; 32, **3**; 63%, **4**). It further indicated that polarity of both the residues decreases, and new amino residues of BSA get buried into the hydrophobic pocket (Supporting Information, Table S5). Furthermore, decrease in the fluorescence intensity of peak 2 (69, **1**; 75, **2**; 36, **3**; 67% **4**) suggested extension of the polypeptide backbone to greater extent and BSA conformational changes. Variation in the fluorescence intensity for both peaks 1 and 2 revealed that interaction between BSA and **1**−**4** leads to changes in both tyrosine and tryptophan residues, microenvironment polarity of amino residues, and conformation of the BSA.

Electrochemical Studies. The cyclic and differential pulse voltammograms for **1**−**4** (MeCN, *c*; 100 μM) are depicted in Figure 9 (Supporting Information, Figures S16−S18), and resulting data are summarized in Supporting Information, Table S6. The complexes under study exhibited two distinct irreversible oxidation waves in the range 0.0−1.4 V. The wave associated with dpm/dpm$^+$ redox process appeared at lower (E_{pa} = 0.807, **1**; 0.777, **2**; 0.695, **3**; 0.679 V, **4**) while those due to metal based oxidations at higher potential (E_{pa} = 0.956, Ru^{2+}/Ru^{3+}, **1**; 0.985, Ru^{2+}/Ru^{3+}, **2**; 0.899, Rh^{3+}/Rh^{4+}, **3**; 0.851 V, Ir^{3+}/Ir^{4+}, **4**).[9d,13,45] Following the trends observed in CV, the DPV of respective complexes displayed peaks assignable to dpm/dpm$^+$ (E_{pa}, 0.757, **1**; 0.750, **2**; 0.704, **3**; and 0.683 V, **4**), and metal based redox processes (0.909, Ru^{2+}/Ru^{3+}, **1**; 0.930, Ru^{2+}/Ru^{3+}, **2**; 0.884, Rh^{3+}/Rh^{4+}, **3**; 0.873 V, Ir^{3+}/Ir^{4+}, **4**). Notably, redox waves were not observed in the cathodic potential window.

Considering the redox active sites it was realized that these complexes may exhibit considerable alteration in their redox properties in presence of DNA. To investigate the binding of complexes with CT DNA, electrochemical titrations (CV and DPV) have been performed. Upon addition of 0.1 μM CT DNA to a solution of **2** the oxidative wave corresponding to dpm/dpm$^+$ couple (E_{pa}, 0.777 V) showed a positive potential shift and an increase in the current intensity (E_{pa}, 0.851 V; ΔE_{pa}, 0.074 V, ΔI, 13%). However, metal based redox couple (Ru^{2+}/Ru^{3+}) displayed weakening (E_{pa}, 0.985 V) and an appreciable decrease in the current intensity (ΔI 78%). In presence of higher concentrations of CT DNA (0.2−1.0 μM) the wave due to dpm/dpm$^+$ couple exhibited additional positive potential shift (E_{pa}, 0.896 V; ΔE_{pa}, 0.119 V, ΔI 68%), while metal based wave Ru^{2+}/Ru^{3+} completely vanished. Appreciable changes in dpm/dpm$^+$ and Ru^{2+}/Ru^{3+} based redox couples clearly indicated some interaction between **2** and CT DNA.

The differential pulse voltammogrm (DPV) of complex **2** followed an analogous pattern in presence of CT DNA (0.1 μM). Positive potential shift of the peak due to dpm/dpm$^+$ (E_{pa}, 0.776 V; ΔE_{pa}, 0.026 V, ΔI, 10%) followed an increase in the current intensity, while the peak associated with the Ru^{2+}/Ru^{3+} (E_{pa}, 0.930 V) redox couple diluted with a substantial decrease in the current intensity (ΔI, 80%). An increase in the concentration of CT DNA (0.2−1.0 μM) led to additional positive potential shift for the peak due to dpm/dpm$^+$ (E_{pa}, 0.833 V; ΔE_{pa}, 0.088 V, ΔI, 10%), while the one due to Ru^{2+}/Ru^{3+} disappeared (Figure 10). It may be due to formation of a new species between complex **2** and CT DNA. The complex **1** followed the similar trends under analogous conditions.

The oxidative waves due to dpm/dpm$^+$ and Rh^{3+}/Rh^{4+} redox couples in complex **3** displayed positive potential shift with a concomitant decrease in the current intensity (E_{pa} 0.708, ΔE_{pa}, 0.013 V, ΔI, 11%; dpm/dpm$^+$; E_{pa} 0.929, ΔE_{pa}, 0.030 V, ΔI, 10%, Rh^{3+}/Rh^{4+}) upon addition of CT DNA (0.1 μM). An increase in the concentration of CT DNA (0.2−1.0 μM) led to additional anodic shift for both waves and a decrease in the current intensity (E_{pa}, 0.746, ΔE_{pa}, 0.051 V, ΔI, 52%; dpm/dpm$^+$ and E_{pa} 1.005, ΔE_{pa}, 0.121 V, ΔI, 44%; Rh^{3+}/Rh^{4+}). Complex **4** exhibited an analogous pattern in the presence of CT DNA. Differential pulse voltammogram of **3** exhibited an anodic shift with attendant decrease in the current intensity upon addition of 0.1 μM CT DNA for both the peaks assignable to dpm/dpm$^+$ and Rh^{3+}/Rh^{4+} at E_{pa}, 0.704 and 0.884 V (E_{pa} 0.713 V; ΔE_{pa}, 0.009 V, ΔI 9%, dpm/dpm$^+$; E_{pa} 0.896, ΔE_{pa}, 0.012 V, ΔI 9%, Rh^{3+}/Rh^{4+}). Increasing the concentration of CT DNA (0.2−1.0 μM) led to a positive potential shift and decrease in the current intensity (E_{pa}, 0.754, ΔE_{pa}, 0.050 V, ΔI 47%, dpm/dpm$^+$; 0.916, ΔE_{pa}, 0.032 V, ΔI 50%; Rh^{3+}/Rh^{4+}) (Supporting Information, Figure S17). Complex **4**

dx.doi.org/10.1021/ic401662d | *Inorg. Chem.* 2013, 52, 13984−13996

exhibited an analogous pattern under similar conditions (Supporting Information, Figure S18).

The electrochemical studies indicated that **1** and **2** interact with CT DNA in a slightly different manner relative to **3** and **4**; this difference in the interaction mode may be related to the oxidation state of the metal ions. The results from electrochemical studies are consistent with spectra especially absorption titration studies and indicate strong interaction between **1**−**4** and CT DNA. Cytotoxicity of the complexes can be correlated with the redox potential.[46] On the basis of electrochemical data cytotoxicity of **1**−**4** can be arranged in the order **4** > **3** > **2** > **1** (E_{pa} = 0.807, **1**; 0.777, **2**; 0.695, **3**; and 0.679 V, **4**).

Partition Coefficient Determination. Lipophilicity plays an important role in the design and development of drugs and their absorption, distribution, metabolism, and elimination.[47] Log *P* is generally used for estimation of the lipophilicity in biphasic system (*n*-octanol/water) owing to comparable environment in biological membranes.[21] To have deep insight into permeation behavior of the complexes across cell membranes, partition coefficients, *P*, have been evaluated.[48,49] The calculated log *P* values (Supporting Information, Table S7) are consistent with the literature reports.[50] A comparison of the partition coefficients (log *P*) for the complexes revealed that their lipophilicity lies in the order **2** > **1** > **4** > **3**. It may be ascribed to enhanced phenyl substitution in **2** relative to **1**, and variation of the metal center in **3** and **4**. Cytotoxicity of the complexes increases with an increase in lipophilicity and is consistent with the results obtained from MTT assay.

Molecular Docking with DNA. To elucidate the mode of interaction and binding affinity, docking studies have been performed on B-DNA (PDB ID: 1BNA) in presence of **1**−**4**. The study revealed that complexes under investigation interact with DNA via an electrostatic mode involving outside edge stacking interaction with oxygen atom of the phosphate backbone. The planarity of the dipyrrin core is compatible for strong $\pi-\pi$ stacking interactions and a better match of the complexes inside the DNA strands. From the ensuing docked structures it is clear that **1**−**4** fits well into the minor groove of the targeted DNA and G−C rich region stabilized by van der Waals interaction and hydrophobic contacts (Figure 11, Supporting Information, Figure S19−S21).[51]

Relative binding energy of the docked structures was found to be −264.05, **1**; −265.32, **2**; −260.93, **3**; and −262.34 eV, **4**. These are consistent with the spectral studies and indicated that **2** has greater binding affinity relative to other complexes.

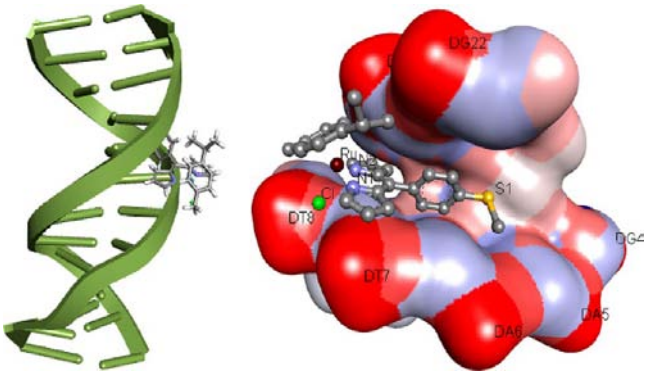

Figure 11. Molecular docked model of complex **2** with DNA (PDB ID: 1BNA).

Overall results suggested that there is good correlation between spectroscopic results and molecular modeling.

Molecular Docking with HSA. To ascertain the binding mode of the complexes **1**−**4** with the most probable site of the Human Serum Albumin (HSA), molecular docking studies have been performed. The HSA was chosen over BSA to obtain a clearer idea about the human protein binding interactions. Structural studies have shown that HSA consists of three homologous domains (denoted as I, II, and III): I (residues 1−195), II (196−383), and III (384−585). The prime region for interaction of HSA with the complexes is hydrophobic environment of the subdomains IIA and IIIA, corresponding to sites I and II, respectively, and the tryptophan residue (Trp-214, subdomain IIA). The molecular docking pattern of **1**−**4** and HSA indicated that complexes are located within the subdomain IIA hydrophobic cavity.

The data analysis clearly showed that **2** is in close proximity of the hydrophobic residues such as LYS 195, TRP 214, ARG 218, GLN 221, ARG 222, ASN 295, PRO 339, ASP 340, TYR 341, SER 342, VAL 343, ALA 443, LYS 444, PRO 447, CYS 448, GLU 450, and ASP 451 (within 4 Å) due to hydrophobic interaction between them (Figure 12, Supporting Information,

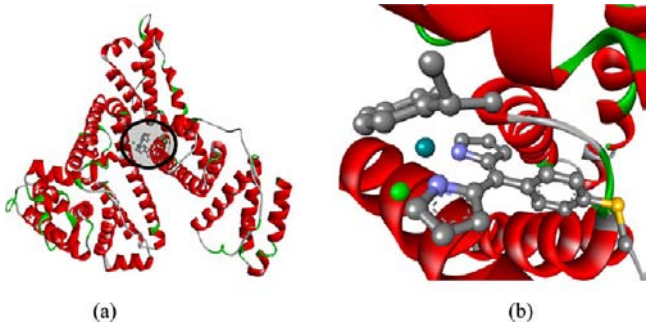

Figure 12. Molecular docked model of **2** located within the hydrophobic pocket of HSA (a) (PDB ID: 1h9z); (b) the interaction mode between **2** (stick) and HSA (cartoon).

Figure S22−S29, Table S8). The electrostatic interactions, hydrogen bonding between **2** and HSA, also stabilized the complex (**2**·HSA) by lowering hydrophilicity and increasing the hydrophobicity.[52] The results obtained from molecular docking studies revealed that the interaction between complex **2** and HSA is dominated by hydrophobic forces. Analogous results were obtained for **1**, **3**, and **4** also. It also provides good structural evidence to explain efficient fluorescence quenching of the BSA fluorophore in presence of **1**−**4**.

Dose Response Curves, Determination of IC_{50} Value. To evaluate the IC_{50} values, MTT assay was analyzed with increasing concentrations of **1**−**4** (range 2−100 μg/mL). It was observed that these exhibit significant inhibitory effect on DL cell proliferation (Supporting Information, Figure S30). Further, a wide variation was observed in the evaluated IC_{50} value (8−10, **1**; 5−10, **2**; 75−100, **3**; and 30−40 μg/mL, **4**). Among these, **2** displayed the lowest IC_{50} value (5−10 μg/mL) indicating its high potency, while **3** exhibited the lowest potency against DL cells. On the basis of the above results, antitumor potency of the complexes can be arranged in order **2** > **1** > **4** > **3**.

Morphological Changes in AO/EtBr Fluorescence Study. Upon exposure to cytotoxic agents the cell death may take place by several modes, and among these apoptosis and

dx.doi.org/10.1021/ic401662d | *Inorg. Chem.* 2013, 52, 13984−13996

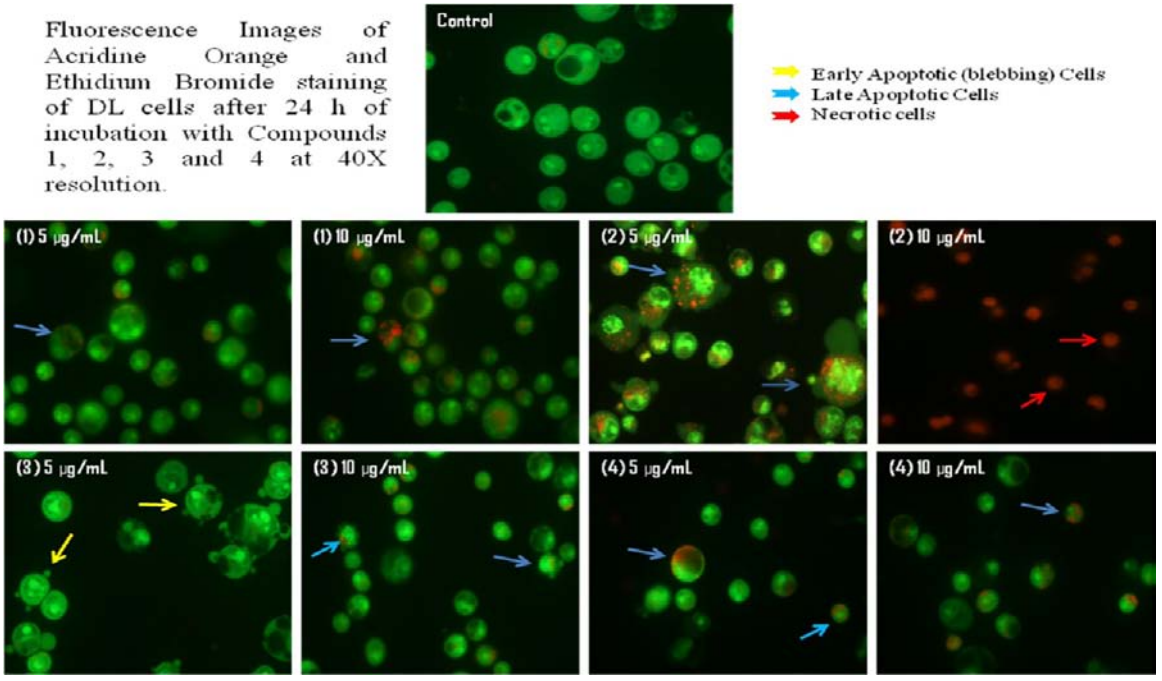

Figure 13. Images of drug treated Dalton's Lymphoma cells after Acridine orange/Ethidium bromide staining after 24 h of treatments with different concentrations. The yellow arrows show early apoptotic cells with blebbing, blue arrows show late apoptosis, and red arrows show necrotic cells.

necrosis are very prominent. Apoptosis or programmed cell death is characterized by cell shrinkage, blebbing of the plasma membrane, and chromatin condensation. To investigate the morphological changes AO/EtBr fluorescence staining was performed and resulting images of the control and treated DL cells are depicted in Figure 13. In this figure yellow arrows show early apoptotic DL cells with membrane blebbing which is seen at lower doses of the compounds **2** and **3**, and blue arrows exhibit late apoptotic cells with chromatin aggregation, that is, highly condensed chromatin. These are the characteristic features of apoptotic cells and quite different from those of the control cells. The red arrow(s) show necrotic cells which are observed at high doses (10 μg/mL) of the compound **2**. Overall results indicate that **1**, **3**, and **4** induce apoptosis at lower as well as higher dose whereas **2** favors apoptosis at lower concentration (2 μg/mL, Supporting Information, Figure S31), but induces necrosis at higher dose.

Apoptotic Study with DNA Ladder Assay. One of the characteristic features of the apoptotic cells is DNA fragmentation, which is considered as biochemical property of the apoptosis.[53] A typical DNA ladder pattern was observed for all the complexes (Figure 14) except **2** which does not show ladder formation at higher doses (5/10 μg/mL; lane 7 and 8). Further, DNA isolated from control DL cells did not show any ladder (Lane 2) formation relative to DNA isolated from the treated DL cells. This study clearly suggested that the complexes under investigation promote apoptosis in DL cells. Further, the observed DNA ladder pattern indicated apoptotic cell death and supports our assumption regarding antitumor activity.

The antitumor agents, synthetic or natural, which can modulate apoptosis or cause cell cycle inhibition or both, affect the steady state of the cell population and are helpful in administration of uncontrolled metastatic cell growth. Most of the existing anticancer drugs exhibit cytotoxicity and induce apoptosis in susceptible cells. Apoptotic cell death is

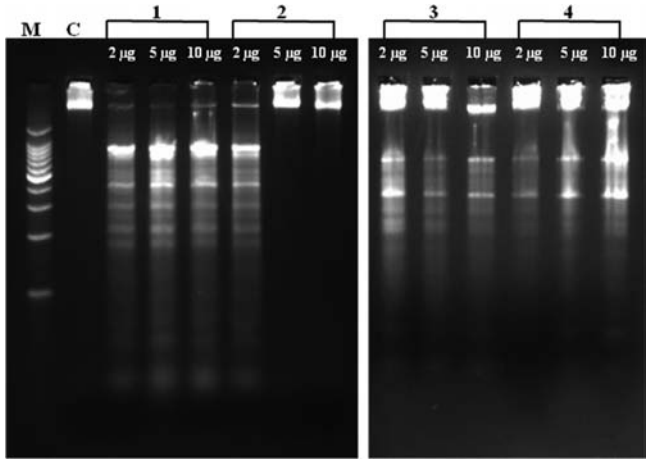

Figure 14. DNA ladder assay, DL cells were treated in culture medium with different concentrations of compounds (in μg/mL) for 24 h and DNA was isolated. DNA from different samples were loaded in each lane and subjected to 1.8% agarose gel electrophoresis.

characterized by nuclear morphology and oligonucleosomal DNA fragments. Present study shows that **1**–**4** significantly induce apoptosis in DL cells. The fluorescence microscopy revealed morphological changes like membrane blebbing, cell shrinkage and nuclear condensation in treated DL cells, whereas these were absent in control DL cells. The fluorescence studies supported occurrence of apoptopic cell death in the presence of these complexes. Among these, **2** exhibited higher toxicity at very low concentration (IC_{50} value; 10 μg/mL) relative to other complexes. MTT assay, fluorescence staining, and DNA ladder pattern strongly support that the complexes under investigation induce apoptotic cell death and may be used as potential anticancer agents.

dx.doi.org/10.1021/ic401662d | *Inorg. Chem.* 2013, 52, 13984–13996

CONCLUSIONS

In conclusion, through the present work new heteroleptic dipyrrinato complexes based on Ru(II), Rh(III), and Ir(III) (**1**−**4**) containing 5-(4-methylthiophenyl)dipyrromethene (4-mtdpm) have been described. Various physicochemical techniques demonstrated that these effectively bind with DNA through intercalative/electrostatic interactions. These also interact with protein (BSA) which has been supported by UV/vis, fluorescence, synchronous and 3D fluorescence spectroscopy. Binding of the complexes through minor DNA groove and protein through the hydrophobic residues such as TRP 214, ARG 218, GLN 221, ARG 222, ASN 295, PRO 339, ASP 340, TYR 341 *etc*. situated within subdomain IIA cavity has been further supported by molecular docking studies. *In vitro* anticancer activity of the complexes shows better cytotoxicity, prominent morphological changes, and better to activate endonuclease for DNA cleavage. The complex **2** exhibited high cytotoxicity (IC_{50} value; 5−10 μg/mL) and induced blebbing even at very low concentrations (2 μg/mL). The complexes presented herein exhibit considerably improved biological activity in comparison to previous report and the results may be useful in understanding the mechanism of interactions of complexes with serum albumin, DNA and also useful in the development of new anticancer agents.

ASSOCIATED CONTENT

Supporting Information

CCDC deposition No. 928847 (**3**) contains the supplementary crystallographic data for this paper. In addition, Tables S3−S8 and Figures S1−S31 contain ^{1}H and ^{13}C NMR, UV/vis, fluorescence titration curves, CV and DPV, ESI-MS and docked model are provided. This material is available free of charge via the Internet at http://pubs.acs.org.

AUTHOR INFORMATION

Corresponding Author

*E-mail: dspbhu@bhu.ac.in. Phone: + 91 542 6702480. Fax: + 91 542 2368174.

Notes

The authors declare no competing financial interest.

ACKNOWLEDGMENTS

The authors thank the "Council of Scientific and Industrial Research, New Delhi" for financial assistance through the Scheme HRDG 01 (2361)/10/EMR-II) and for the award of a Junior Research Fellowship to RKG (No. 09/013(0210)/2009-EMR-I). We are also thankful to the Head, Departments of Chemistry and Zoology, Faculty of Science, Banaras Hindu University, Varanasi (U.P.) India, for extending laboratory facilities and National Institute of Advanced Industrial Science and Technology (AIST), Osaka, Japan for providing single crystal X-Ray data and the Centre for Bioinformatics, Banaras Hindu University, Varanasi for providing *in silico* facilities.

REFERENCES

(1) (a) Globocan **2008**; International Agency for Research on Cancer: Lyon, France, 2010. (b) Ma, X.; Yu, H. *Yale J. Biol Med.* **2006**, *79*, 85. (c) Witschi, H. *Toxicol. Sci.* **2001**, *64*, 4.

(2) (a) Innocenti, F.; Ratain, M. J. *Eur. J. Cancer* **2002**, *38*, 639. (b) Lee, W.; Lockhart, A. C.; Kim, R. B.; Rothenberg, M. L. *Oncologist* **2005**, *10*, 104.

(3) (a) Rijt, S. H. V.; Sadler, P. J. *Drug Discovery Today* **2009**, *14*, 1089. (b) Hernandes, M. Z.; de S Pontes, F. J.; Coelho, L. C.; Moreira, D. R.; Pereira, V. R.; Leite, A. C. *Curr. Med. Chem.* **2010**, *17*, 3739. (c) Bruijnincx, P. C.; Sadler, P. J. *Curr. Opin. Chem. Biol.* **2008**, *12*, 197. (d) Raman, N.; Jeyamurugan, R.; Sakthivel, A.; Mitu, L.; Spectrochim Acta, A. *Mol. Biomol. Spectrosc.* **2010**, *75*, 88.

(4) (a) Cepeda1, V.; Fuertes, M. A.; Castilla, J.; Alonso, C.; Quevedo, C.; Perez, J. M. *Anti-Cancer Agents Med. Chem.* **2007**, *7*, 3. (b) Giaccone, G.; Herbst, R. S.; Manegold, C.; Scagliotti, G.; Rosell, R.; Miller, V. *J. Clin. Oncol.* **2004**, *22*, 777.

(5) (a) Gasser, G.; Ott, I.; Metzler-Nolte, N. *J. Med. Chem.* **2011**, *54*, 3. (b) Jakupec, M. A.; Galanski, M.; Arion, V. B.; Hartinger, C. G.; Keppler, B. K. *Dalton Trans.* **2008**, *2*, 183. (c) Dyson, P. J.; Sava, G. *Dalton Trans.* **2006**, 1929. and references therein. (d) Desoize, B. *Anticancer Res.* **2004**, *24*, 1529.

(6) (a) Clarke, M. J. *Coord. Chem. Rev.* **2003**, *236*, 209. (b) Smitha, G. S.; Therrien, B. *Dalton Trans.* **2011**, *40*, 10793.

(7) (a) Bratsos, I.; Jedner, S.; Gianferrara, T.; Alessio, E. *Chimia* **2007**, *61*, 692. (b) Lentz, F.; Drescher, A.; Lindauer, A.; Henke, M.; Hilger, R. A.; Hartinger, C. G.; Scheulen, M. E.; Dittrich, C.; Keppler, B. K.; Jaehde, U. *Anti-Cancer Drugs* **2009**, *20*, 97. (c) Gianferrara, T.; Bratsos, I.; Alessio, E. *Dalton Trans.* **2009**, 7588. (d) Suss-Fink, G. *Dalton Trans.* **2010**, *39*, 1673.

(8) (a) Ginzinger, W.; Muhlgassner, G.; Arion, V. B.; Jakupec, M. A.; Roller, A.; Galanski, M.; Reithofer, M.; Berger, W.; Keppler, B. K. *J. Med. Chem.* **2012**, *55*, 3398.

(9) (a) Bruijnincx, P. C. A.; Sadler, P. J. *Adv. Inorg. Chem.* **2009**, *61*, 1. (b) Singh, S. K.; Joshi, S.; Singh, A. R.; Saxena, J. K.; Pandey, D. S. *Inorg. Chem.* **2007**, *46*, 10869. (c) Peacock, A. F. A.; Sadler, P. J. *Chem.—Asian J.* **2008**, *3*, 1890. (d) Gupta, R. K.; Pandey, R.; Sharma, G.; Prasad, R.; Koch, B.; Srikrishna, S.; Li, P.-Z.; Xu, Q.; Pandey, D. S. *Inorg. Chem.* **2013**, *52*, 3687.

(10) Esposito, B. P.; Najjar, R. *Coord. Chem. Rev.* **2002**, *232*, 137.

(11) (a) Sielecki, T. M.; Boylan, J. F.; Benfield, P. A.; Trainor, G. L. *J. Med. Chem.* **1999**, *43*, 1. (b) Zang, Z.; Jin, L.; Qian, X.; Wei, M.; Wang, Y.; Wang, J.; Yang, Y.; Xu, Q.; Xu, Y.; Liu, F. *ChemBioChem.* **2007**, *8*, 113.

(12) (a) Siu, P. K. M.; Ma, D. L.; Che, C. M. *Chem. Commun.* **2005**, 1025.

(13) Dougan, S. J.; Habtemariam, A.; McHale, S. E.; Parsons, S.; Sadler, P. J. *Proc. Natl. Aacad. Sci. U.S.A.* **2008**, *105*, 11628. (2) Giannini, F.; Suss-Fink, G.; Furrer, J. *Inorg. Chem.* **2011**, *50*, 10552. (3) Gianferrara, T.; Bratsos, I.; Alessio, E. *J. Biol. Inorg. Chem.* **2012**, *17*, 951.

(14) (a) Wood, T. E.; Thompson, A. *Chem. Rev.* **2007**, *107*, 1831. (b) Baudron, S. A. *CrystEngComm.* **2010**, *12*, 2288. (c) Pogozhev, D.; Baudron, S. A.; Hosseini, M. W. *CrystEngComm* **2010**, *12*, 2238. (d) Murphy, D. L.; Malachowski, M. R.; Campana, C.; Cohen, S. M. *Chem. Commun.* **2005**, 5506. (e) Kilduff, B.; Pogozhev, D.; Baudron, S. A.; Hosseini, M. W. *Inorg. Chem.* **2010**, *49*, 1123. (f) Mendoza, D. S.; Baudron, S. A.; Hosseini, M. W. *Inorg. Chem.* **2008**, *47*, 766. (g) Telfer, S. G.; Wuest, J. D. *Cryst. Growth Des.* **2009**, *9*, 1923. (h) Telfer, S. G.; Wuest, J. D. *Chem. Commun.* **2007**, 3166. (i) Yadav, M.; Singh, A. K.; Pandey, D. S. *Organometallics* **2009**, *28*, 4713. (j) Yadav, M.; Singh, A. K.; Maiti, B.; Pandey, D. S. *Inorg. Chem.* **2009**, *48*, 7593−9929. (k) Yadav, M.; Kumar, P.; Pandey, D. S. *Polyhedron* **2010**, *29*, 791. (l) Yadav, M.; Singh, A. K.; Pandey, D. S. *J. Organomet. Chem.* **2011**, *696*, 758. (m) Gupta, R. K.; Pandey, R.; Singh, R.; Srivastava, N.; Maiti, B.; Saha, S.; Li, P.; Xu, Q.; Pandey, D. S. *Inorg. Chem.* **2012**, *51*, 8916.

(15) (a) Wagner, R. W.; Lindsey, J. S. *J. Am. Chem. Soc.* **1994**, *116*, 9759. (b) Koepf, M.; Trabolsi, A.; Elhabiri, M.; Wytko, J. A.; Paul, D.; Gary, A. M. A.; Weiss, J. *Org. Lett.* **2005**, *7*, 1279. (c) Maeda, H.; Hasegawa, M.; Hashimoto, T.; Kakimoto, T.; Nishio, S.; Nakanishi, T. *J. Am. Chem. Soc.* **2006**, *128*, 10024.

(16) (a) Goldie, H.; Felix, M. D. *Cancer Res.* **1951**, *11*, 73. (b) Wang, X.; Guo, Z. *Anti-Cancer Agents Med. Chem.* **2007**, *7*, 19. (c) Jacob, C.; Giles, G. I.; Giles, N. M.; Sies, H. *Angew. Chem., Int. Ed.* **2003**, *42*, 4742.

(17) (a) Suda, Y.; Arano, A.; Fukui, Y.; Koshida, S.; Wakao, M.; Nishimura, T.; Kusumoto, S.; Sobel, M. *Bioconjugate Chem.* **2006**, *17*,

1125. (b) Esposito, B. P.; Najjar, R. *Coord. Chem. Rev.* **2002**, *232*, 137. (c) Mahon, A. B.; Arora, P. S. *Chem. Commun.* **2012**, *48*, 1 416. (d) Stoffregen, S. A.; Griffin, A. K. K.; Kostic, N. M. *Inorg. Chem.* **2005**, *44*, 8899.
(18) Perrin, D. D.; Armango, W. L. F.; Perrin, D. R. *Purification of laboratory Chemicals*; Pergamon: Oxford, U.K., 1986.
(19) (a) Bennett, M. A.; Smith, A. K. *J. Chem. Soc., Dalton Trans.* **1974**, 233. (b) Bennett, M. A.; Huang, T. N.; Matheson, T. W.; Smith, A. K. *Inorg. Synth.* **1982**, *21*, 74. (c) Kang, W.; Moseley, K.; Maitlis, P. M. *J. Am. Chem. Soc.* **1969**, *91*, 5970. (d) Ball, R. G.; Graham, W. A. G.; Heinekey, D. M.; Hoyano, J. K.; McMaster, A. D.; Mattson, B. M.; Michel, S. T. *Inorg. Chem.* **1990**, *29*, 2023. (e) White, C.; Yates, A.; Maitlis, P. M. *Inorg. Synth.* **1992**, *29*, 228.
(20) Sheldrick, G. M. *Acta Crystallogr.* **2008**, *A64*, 112.
(21) (a) Spek, A. L. *PLATON, A Multipurpose Crystallographic Tools*; Utrecht University: Utrecht, The Netherlands, 2000. (b) Spek, A. L. *Acta Crystallogr., Sect. A* **1990**, *46*, C31.
(22) (a) *OECD, Guidelines for Testing of Chemicals*. OECD: Paris, France, 1995; Vol. *107*. (b) Graham, L. P. *An Introduction to Medicinal Chemistry*; Oxford University Press: Oxford, U.K., 1995. (c) Li, L.; Cao, W.; Zheng, W.; Fan, C.; Chen, T. *Dalton Trans.* **2012**, *41*, 12766.
(23) Mustard, D.; Ritchie, D. W. *Proteins: Struct. Funct. Bioinf.* **2005**, *60*, 269.
(24) (a) Becke, A. D. *J. Chem. Phys.* **1993**, *98*, 5648. (b) Lee, C. T.; Yang, W. T.; Parr, R. G. *Phys. Rev. B: Condens. Matter Mater. Phys.* **1988**, *37*, 785. (c) Krishnan, R.; Binkley, J. S.; Seeger, R.; Pople, J. A. *J. Chem. Phys.* **1980**, *72*, 650. (d) McClean, A. D.; Chandler, G. S. *J. Chem. Phys.* **1980**, *72*, 5639. (e) Hay, P.; Wadt, W. R. *J. Chem. Phys.* **1985**, *82*, 270. (f) Wadt, W. R.; Hay, P. *J. Chem. Phys.* **1985**, *82*, 284. (g) Hay, P.; Wadt, W. R. *J. Chem. Phys.* **1985**, *82*, 299.
(25) Mosmann, T. J. *J. Immunol. Methods* **1983**, *65*, 55.
(26) McGahon, A. J.; Martin, S. J.; Bissonnette, R. P.; Mahboubi, A.; Shi, Y.; Mogil, R. J.; Nishioka, W. K.; Green, D. R. *Methods Cell Biol.* **1995**, *46*, 153.
(27) Bezabeh, T.; Mowat, M. R. A.; Jarolim, L.; Greenberg, A. H.; Smith, I .C. P. *Cell Death Differ.* **2001**, *8*, 219.
(28) Wyllie, A. H. *Nature* **1980**, *284*, 555.
(29) Kuo, P. L.; Hsu, Y. L.; Chang, C. H.; Lin, C. C. *Cancer Lett.* **2005**, *223*, 293.
(30) (a) Do, L.; Halper, S. R.; Cohen, S. M. *Chem. Commun.* **2004**, 2662.
(31) (a) Prasad, K. T.; Therrein, B.; Rao, K. M. *J. Organomet. Chem.* **2010**, *695*, 1375. (b) Gupta, G.; Gloria, S.; Therrien, B.; Das, B.; Rao, K. M. *J. Organomet. Chem.* **2011**, *696*, 702. (c) Hall, J. D.; McLean, T. M.; Smalley, S. J.; Waterland, M. R.; Telfer, S. G. *Dalton Trans.* **2010**, *39*, 437. (d) Hanson, K.; Tamayo, A.; Diev, V. V.; Whited, M. T.; Djurovich, P. I.; Thompson, M. E. *Inorg. Chem.* **2010**, *49*, 6077. (e) Bronner, C.; Baudron, S. A.; Hosseini, M. W. *Inorg. Chem.* **2010**, *49*, 8659.
(32) (a) Tanious, A. F.; Ding, D. Y.; Patrick, D. A.; Bailly, C.; Tidwell, R. R.; Wilson, W. D. *Biochemistry* **2000**, *39*, 12091. (b) Zhong, C. Y.; Zhao, J.; Wu, Y. B.; Yin, C. X.; Yang, P. *J. Inorg. Biochem.* **2007**, *101*, 10.
(33) (a) Zhang, Q. L.; Liu, J. G.; Chao, H.; Xue, G. Q.; Ji, L. N. *J. Inorg. Biochem.* **2001**, *83*, 49. (b) Liu, Z. C.; Wang, B. D.; Li, B.; Wang, Q.; Yang, Z. Y.; Li, T. R.; Li, Y. *Eur. J. Med. Chem.* **2010**, *45*, 5353.
(34) (a) Mancin, F.; Scrimin, P.; Tecilla, P.; Tonellato, U. *Chem. Commun.* **2005**, 2540. (b) Tjioe, L.; Meininger, A.; Joshi, T.; Spiccia, L.; Graham, B. *Inorg. Chem.* **2011**, *50*, 4327.
(35) (a) Carter, M. T.; Rodriguez, M.; Bard, A. J. *J. Am. Chem. Soc.* **1989**, *111*, 8901. (b) McGhee, J. D.; Hippel, P. H. V. *J. Mol. Biol.* **1974**, *86*, 469. (c) Nelson, D. L.; Cox, M. M. *Lehninger Principles of Biochemistry*, 4th ed.; W. H. Freeman and Company: New York, 2005; p 516.
(36) (a) Herebian, D.; Sheldrick, W. S. *J. Chem. Soc., Dalton Trans.* **2002**, 966.
(37) (a) Long, E. C.; Barton, J. K. *Acc. Chem. Res.* **1990**, *23*, 271. (b) Pasternack, R. F.; Gibbs, E. J.; Villafranca, J. J. *Biochemistry* **1983**, *22*, 251.
(38) (a) Liu, Z. C.; Wang, B. D.; Yang, Z. Y.; Li, Y.; Qin, D. D.; Li, T. R. *Eur. J. Med. Chem.* **2009**, *44*, 4477. (b) Meyer-Almes, F. J.; Porschke, D. *Biochemistry* **1993**, *32*, 4246. (c) Howe, G. M.; Wu, K. C.; Bauer, W. R. *Biochemistry* **1976**, *19*, 339.
(39) (a) Ramachandran, E.; Raja, D. S.; Bhuvanesh, N. S. P.; Natarajan, K. *Dalton Trans.* **2012**, *41*, 13308. (b) Raja, D. S.; Bhuvanesh, N. S. P.; Natarajan, K. *Dalton Trans.* **2012**, *41*, 4365.
(40) (a) Raja, D. S.; Paramaguru, G.; Bhuvanesh, N. S. P.; Reibenspies, J. H.; Renganathan, R.; Natarajan, K. *Dalton Trans.* **2011**, *40*, 4548. (b) Raja, D. S.; Bhuvanesh, N. S. P.; Natarajan, K. *Eur. J. Med. Chem.* **2011**, *46*, 4584. (c) Eftink, M. R.; Ghiron, C. A. *J. Phys. Chem.* **1976**, *80*, 486.
(41) Miller, J. N. *Proc. Anal. Div. Chem. Soc.* **1979**, *16*, 203.
(42) Tang, J. H.; Luan, F.; Chen, X. G. *Bioorg. Med. Chem.* **2006**, *49*, 3210.
(43) Bernhardt, P. V.; Sharpe, P. C.; Islam, M.; Lovejoy, D. B.; Kalinowski, D. S.; Richardson, D. R. *J. Med. Chem.* **2009**, *52*, 407.
(44) (a) Han, X.; Mei, P.; Liu, Y.; Xiao, Q.; Jiang, F.; Li, R. *Spectrochim. Acta, Part A* **2009**, *74*, 781. (b) Tong, J. Q.; Tian, F. F.; Li, Q.; Li, L. L.; Xiang, C.; Liu, Y.; Dai, J.; Jiang, F. L. *Photochem. Photobiol. Sci.* **2012**, *11*, 1868.
(45) (a) Yu, L.; Muthukumaran, K.; Sazanovich, I. V.; Kirmaier, C.; Hindin, E.; Diers, J. R.; Boyle, P. D.; Bocian, D. F.; Holten, D.; Lindsey, J. S. *Inorg. Chem.* **2003**, *42*, 6629. (b) Goze, C.; Ulrich, G.; Ziessel, R. *J. Org. Chem.* **2007**, *72*, 313.
(46) (a) Hall, M. D.; Hambley, T. W. *Coord. Chem. Rev.* **2002**, *232*, 49. (b) Milhazes, N.; Cunha-Oliveira, T.; Martins, P.; Garrido, J.; Oliveira, C.; Rego, A. C.; Borges, F. *Chem. Res. Toxicol.* **2006**, *19*, 1294.
(47) (a) Yang, Y.; Engkvist, O.; Llinaas, A.; Chen, H. *J. Med. Chem.* **2012**, *55*, 3667. (b) Theil, F. P.; Guentert, T. W.; Haddad, S.; Poulin, P. *Toxicol. Lett.* **2003**, *138*, 29.
(48) (a) Pignatello, R.; Musumeci, T.; Basile, L.; Carbone, C.; Puglisi, G. *J. Pharm. Bioallied Sci.* **2011**, *3*, 4. (b) Fresta, M.; Guccione, S.; Beccari, A. R.; Furneric, P. M.; Puglisi, G. *Bioorg. Med. Chem.* **2002**, *10*, 3871.
(49) (a) Fatouros, D. G.; Karpf, D. M.; Nielsen, F. S.; Mullertz, A. *Ther. Clin. Risk Manage.* **2007**, *3*, 591. (b) Martins, S.; Sarmento, B.; Ferreira, D. C.; Souto, E. B. *Int. J. Nanomed.* **2007**, *2*, 595.
(50) (a) Liu, Z.; Habtemariam, A.; Pizarro, A. M.; Fletcher, S. A.; Kisova, A.; Vrana, O.; Salassa, L.; Bruijnincx, P. C. A.; Clarkson, G. J.; Brabec, V.; Sadler, P. J. *J. Med. Chem.* **2011**, *54*, 3011. (b) Aguirre, J. D.; Angeles-Boza, A. M.; Chouai, A.; Pellois, Jean-P.; Turro, C.; Dunbar, K. R. *J. Am. Chem. Soc.* **2009**, *131*, 11353. (c) Vock, C. A.; Renfrew, A. K.; Scopelliti, R.; Jeanneret, L. J.; Dyson, P. J. *Eur. J. Inorg. Chem.* **2008**, 1661.
(51) Tabassum, S.; Zaki, M.; Afzal, M.; Arjmand, F. *Dalton Trans.* **2013**, *42*, 10029.
(52) (a) Filosa, R.; Peduto, A.; Micco, S. D.; Caprariis, P. D.; Festa, M.; Petrella, A.; Capranico, G.; Bifulco, G. *Bioorg. Med. Chem.* **2009**, *17*, 13. (b) Tabassum, S.; Asbahy, W. M. A.; Afzal, M.; Arjmand, F.; Khan, R. H. *Mol. BioSyst.* **2012**, *8*, 2424.
(53) Zhang, J.; Xu, M. *Cell Biol.* **2002**, *12*, 84.